

Learning-based Online Optimization for Autonomous Mobility-on-Demand Fleet Control

Kai Jungel¹, Axel Parmentier², Maximilian Schiffer³, and Thibaut Vidal⁴

¹TUM School of Management, Technical University of Munich, 80333 Munich, Germany
kai.jungel@tum.de

²CERMICS, École des Ponts, Marne-la-Vallée, France
axel.parmentier@enpc.fr

³TUM School of Management & Munich Data Science Institute,
Technical University of Munich, 80333 Munich, Germany
schiffer@tum.de

⁴CIRRELT & SCALE-AI Chair in Data-Driven Supply Chains, Department of Mathematics and Industrial
Engineering, École Polytechnique de Montréal, Montréal, Canada,
Department of Computer Science, Pontifical Catholic University of Rio de Janeiro, Rio de Janeiro, Brazil
thibaut.vidal@cirrelt.ca

Abstract

Autonomous mobility-on-demand systems are a viable alternative to mitigate many transportation-related externalities in cities, such as rising vehicle volumes in urban areas and transportation-related pollution. However, the success of these systems heavily depends on efficient and effective fleet control strategies. In this context, we study online control algorithms for autonomous mobility-on-demand systems and develop a novel hybrid combinatorial optimization enriched machine learning pipeline which learns online dispatching and rebalancing policies from optimal full-information solutions. We test our hybrid pipeline on large-scale real-world scenarios with different vehicle fleet sizes and various request densities. We show that our approach outperforms state-of-the-art greedy, and model-predictive control approaches with respect to various KPIs, e.g., by up to 17.1% and on average by 6.3% in terms of realized profit.

Keywords: mobility-on-demand, structured learning, online algorithm, central control

1. Introduction

Growing urbanization leads to rising traffic volumes in urban areas and challenges the sustainability and economic efficiency of today’s urban transportation systems. In fact, transportation systems’ externalities, such as congestion and local emissions, can significantly damage public health and pose a growing threat to our environment (Levy et al. 2010, Schrank et al. 2019). Moreover, private cars currently require considerable space for parking and driving in urban areas.

Recent progress in autonomous driving and 5G technology has led to crucial advances towards enabling autonomous mobility-on-demand (AMoD) systems (White 2020), which can contribute to mitigating many of the aforementioned challenges in the coming years. An AMoD system consists of a centrally-controlled fleet of self-driving vehicles serving on-demand ride requests (Pavone 2015). To manage the fleet, a central controller dispatches ride requests to vehicles in order to transport customers between their origin and destination. The central controller may further relocate idle vehicles to better match future demand, e.g., in high-demand areas. An AMoD system has many advantages over current conventional ride-hailing systems. Among others, it permits centralized control and therefore enables system-optimal dispatching decisions. Moreover, it allows for a high utilization of vehicles which results from rebalancing actions. However, the utilization of an AMoD system depends on its efficient operation, i.e., system optimal online dispatching and rebalancing of the vehicle fleet. Designing such an efficient control algorithm for AMoD systems faces two major challenges. First, the underlying planning problem is an online control problem, i.e., the central controller must take dispatching and rebalancing decisions under uncertainty without knowing future ride requests. Second, the scalability of the control mechanism for large-scale applications can be computationally challenging as dozens of thousands of requests will need to be satisfied every hour in densely populated areas.

Against this background, we develop a novel family of scalable online-control policies that receive an online AMoD system state as input and return dispatching and rebalancing actions for the AMoD fleet. Specifically, we encode these online control policies via a hybrid combinatorial optimization (CO) enriched machine learning (ML) pipeline. The rationale of this hybrid CO-enriched ML pipeline is to transform the online AMoD system state into a combinatorial dispatching problem, and to learn the parameterization of this dispatching problem from optimal full-information solutions, based on historical data. As a result, the solution of the dispatching problem imitates optimal full-information solutions and leads to anticipative online dispatching and rebalancing actions.

1.1. Related Work

Our work contributes to two different research streams. From an application perspective, it connects to vehicle routing and dispatching problems for AMoD systems. From a methodological perspective, it connects to the field of CO-enriched ML. In this section, we first review related works in the field of AMoD systems and refer to Vidal et al. (2020) for a general overview of vehicle routing problems.

Second, we review related works at the intersection of ML and CO, and refer to Bengio et al. (2021) and Kotary et al. (2021) for a general overview.

AMoD Systems. AMoD systems have been studied from a system perspective and from an operational perspective. Studies that focused on the system perspective investigated offline problem settings with full information on all ride requests, addressing research questions related to strategic decision-making and mesoscopic analyses, and are only loosely related to our work. Therefore, we exclude these from our review and refer to Zardini et al. (2022) for a general overview.

This study relates to the operational perspective, specifically to online systems with ride requests entering the system sequentially over time. To solve such an online dispatching problem, classical CO approaches which leverage the combinatorial structure of the problem, as well as ML approaches which learn to account for the uncertain appearance of future ride requests exist. In the context of classical CO, Bertsimas et al. (2019) introduced an online re-optimization algorithm, which iteratively optimizes the dispatching of available vehicles to new ride requests when they enter the system in a rolling-horizon fashion. Other works focused explicitly on relocating unassigned vehicles to areas of high future demand to reduce waiting times for future ride requests (Pavone et al. 2012, Zhang & Pavone 2016, Iglesias et al. 2018, Liu & Samaranayake 2022). As the efficiency of dispatching and rebalancing depends on future ride requests, model-predictive control (Alonso-Mora et al. 2017) and stochastic model-predictive control algorithms (Tsao et al. 2018) have been developed to incorporate information about future ride requests. A complementary stream of research studied similar problems from a deep reinforcement learning (DRL) perspective, explicitly focusing on rebalancing (Jiao et al. 2021, Gammelli et al. 2021, Skordilis et al. 2022, Liang et al. 2022) or non-myopic (anticipative) dispatching (Xu et al. 2018, Li et al. 2019, Tang et al. 2019, Zhou et al. 2019, Sadeghi Eshkevari et al. 2022, Enders et al. 2023).

As can be seen, non-myopic dispatching and rebalancing for AMoD systems has recently been vividly studied. Existing approaches either follow a DRL paradigm to account for uncertain system dynamics, or focus on classical optimization-based (control) approaches that are often extended by a sequential prediction component. However, a truly integrated approach that aims to combine learning and optimization to leverage the advantages of both concepts simultaneously has not been studied so far.

Combinatorial Optimization enriched Machine Learning. In many applications, combinatorial decisions are subject to uncertainty. In this context, various approaches that enrich CO by ML components to account for uncertainty have recently been studied. For example, Donti et al. (2017) proposed an end-to-end learning approach for probabilistic models in the course of stochastic optimization, and Elmachtoub & Grigas (2022) introduced a loss to learn a prediction model for travel times by utilizing the structure of the underlying vehicle routing problem. Closest to our paradigm are approaches to which we can generally refer as CO-enriched ML pipelines (cf. Dalle et al. 2022). In particular, these approaches revolve around the concept of structured learning (SL), a supervised learning methodology with a combinatorial solution space (cf. Nowozin & Lampert 2010), which can be used to enrich CO-algorithms with a prediction component. Parmentier (2021) used structured

learning (SL) to parametrize a computationally tractable surrogate problem such that its solution approximates the solution of a hard combinatorial problem. Using this concept, Parmentier & T'Kindt (2022) solved a single-machine scheduling problem with release dates by transforming it into a computationally tractable scheduling problem without release dates.

These recent works point towards the efficiency of CO-enriched ML when determining approximate solutions for hard-to-solve combinatorial problems. However, it remains an open question whether CO-enriched ML can also successfully be used to derive efficient online control policies, especially in the realm of AMoD systems.

1.2. Contributions

In this paper, we introduce a new state-of-the-art algorithm for large-scale online dispatching and rebalancing of AMoD systems. To reach this goal, we close the research gaps outlined above by introducing a novel family of online control policies, encoded via a hybrid CO-enriched ML pipeline. In a nutshell, this hybrid CO-enriched ML pipeline receives an AMoD system state, transforms it into a combinatorial dispatching problem, parameterizes the dispatching problem by utilizing SL, and solves it to return online dispatching and rebalancing actions. The main rationale of this hybrid CO-enriched ML pipeline is to learn the parametrization of the dispatching problem from optimal full-information solutions for historical data, in such a way that the resulting policy imitates fully-informed dispatching and rebalancing actions.

The contribution of our work is several-fold. First, we present a novel CO-enriched ML pipeline, amenable to derive online control policies, and tailor it to online dispatching and rebalancing for AMoD systems. Second, to establish this pipeline, we show how to solve the underlying CO problem, namely a dispatching and rebalancing problem, in polynomial time. Third, we show how to learn a parametrization for the underlying CO problem based on optimal full-information solutions from historical data using an SL-approach. Fourth, we derive two online control policies, namely a sample-based (SB) approach, and a cell-based (CB) approach, both utilizing our hybrid CO-enriched ML pipeline. Fifth, we present a numerical study based on real-world data to benchmark the encoded policies against current state-of-the-art benchmarks: a greedy policy and a sampling-based receding horizon approach (cf. Alonso-Mora et al. 2017).

Our results show that our learning-based policies outperform a greedy policy with respect to realized profit by up to 17.1% and by 6.3% on average. Moreover, our learning-based policies robustly perform better than a greedy policy across various scenarios, whereas a sampling-based policy oftentimes performs worse than greedy. In general, a sampling-based policy shows an inferior performance compared to our learning-based policies, even in the scenarios where it improves upon greedy. Finally, we show that our learning-based policies yield a good trade-off between anticorrelated key performance indicators, e.g., when maximizing the total profit or the number of served customers, we still obtain a lower distance driven per vehicle compared to policies that show worse performance on the aforementioned quantities.

1.3. Organization

The remainder of this paper is structured as follows. In Section 2, we detail our problem setting. In Section 3, we introduce our hybrid CO-enriched ML pipeline and derive the SL problem to learn an ML-predictor which parameterizes the underlying CO problem. We present a real-world case study in Section 4 and its numerical results in Section 5. Section 6 finally concludes the paper.

2. Problem setting

We study an online vehicle routing problem from the perspective of an AMoD system’s central controller, which steers a homogeneous fleet of self-driving vehicles. The central controller either dispatches vehicles to serve ride requests or rebalances idle vehicles to anticipate future ride requests. Here, a ride request can represent a solitary ride or pooled rides as we assume decisions on pooling requests to be taken at an upper planning level. Accordingly, each ride request demands a mobility service from an origin to a destination location at a certain point in time. The central controller takes decisions according to a discrete time horizon $\{1, \dots, T\}$. We denote the period between the actual decision time t and the subsequent decision time $t + 1$ as system time period $[t, t + 1)$. We consider a set of vehicles \mathcal{V} that serve requests. Each ride request $r \in R$ is a quintuple $r = (o_r, d_r, s_r, a_r, p_r)$ with a pick-up location o_r , a drop-off location d_r , a start time s_r , an arrival time a_r , and its reward p_r . Here, the start time s_r , and the arrival-time a_r are the times when the vehicle reaches the origin o_r and destination d_r of the ride request respectively. Let $\tau(l_1, l_2)$ denote the driving time of a vehicle between two locations l_1 and l_2 . The start time s_r , the arrival time a_r , and the driving time $\tau(l_1, l_2)$ are not subject to the time discretization but are from a continuous time range in \mathbb{R} . If the central controller assigns a ride request to a vehicle, the vehicle has to fulfill this ride request. We refer to a sequence of ride requests that a vehicle fulfills as a *trip*.

System state: At any decision time t , the state $x_{v,t}$ of a vehicle v is a pair $(l_{v,t}, S_{v,t})$ composed of its current location $l_{v,t}$ and a sequence $S_{v,t} = (r_1, r_2, \dots, r_m)$ of unfinished requests which have been assigned to v at the previous decision time $t - 1$. A request r is unfinished when $a_r > t$. In our setting, the sequence of unfinished requests contains $|S_{v,t}| \in \{0, 1\}$ elements as the central controller could only assign requests which started before the decision time t , while in a general setting when the central controller could assign requests which start after the decision time t , the sequence contains $|S_{v,t}| \in \mathbb{N}_0$ elements. The sequence is empty when the vehicle has already fulfilled all assigned requests, which means that the vehicle is idling. Regarding the overall AMoD system state, the state $x_t = (R_t, (x_{v,t})_{v \in V})$ comprises the batch R_t of requests that entered the system between the previous decision time $t - 1$ and t with $s_r \in [t, t + 1)$, as well as the state of each vehicle $v \in \mathcal{V}$.

Feasible decisions: Given the current state of the system x_t , the central controller decides at decision time t which requests $r \in R_t$ to accept and assigns them to vehicles. The central controller

can also rebalance a vehicle after the last request in its trip or when it is idling. A feasible decision $y_{v,t}$ for vehicle v given its current state $x_{v,t} = (l_{v,t}, S_{v,t})$ is a *trip*, i.e., a sequence of requests $\tilde{S}_{v,t} = (r_1, r_2, \dots, r_m, r_{m+1}, \dots, r_n, l)$. This trip $\tilde{S}_{v,t}$ includes the unfinished requests which have already been assigned to v at the previous decision time, i.e., from the sequence $S_{v,t}$, which is then potentially followed by new requests r_{m+1}, \dots, r_n from batch R_t , and may include a final rebalancing location l . A trip satisfies the following *constraints*:

- (i) Each request in a trip does not belong to a trip of another vehicle, meaning $y_v \cap y_{v'} \cap R_t = \emptyset$ for all $v \neq v'$ where $y_v \cap y_{v'} \cap R$ denotes the set of requests in y_v and $y_{v'}$. Note that two vehicles can have the same rebalancing location.
- (ii) For every pair (r_i, r_{i+1}) of successive requests, the vehicle can reach the origin of r_{i+1} on time after r_i , i.e., $a_{r_i} + \tau(d_{r_i, o_{r_{i+1}}}) \leq s_{r_{i+1}}$.
- (iii) If the first request r_1 is new, i.e., $r_1 \in R_t$, then it must be reachable from the current location of the vehicle: $t + \tau(l_{v,t}, o_{r_1}) \leq s_{r_1}$.

We denote by $\mathcal{Y}^v(x_{v,t}, R_t)$ the set of trips available for v given the vehicle state $x_{v,t}$ and the set of new ride requests R_t . Then, the set of feasible dispatching decisions given the current state of the system is

$$\mathcal{Y}(x_t) = \left\{ (y_{v,t})_{v \in V} : y_{v,t} \in \mathcal{Y}^v(x_{v,t}, R_t) \text{ for all } v \in V \right\}.$$

Evolution of the system: Once the central controller dispatches the decision y_t from decision time t , the system evolves until $t + 1$. Each vehicle v drives along its trip. If a vehicle completes its trip before $t + 1$, it idles. If the vehicle does not reach its rebalancing location l before $t + 1$, it starts idling at $t + 1$ and awaits the next operator's decision. We can therefore deduce from $y_{v,t}$ its position $l_{v,t+1}$ at $t + 1$. The system removes all requests from R_t that were assigned at time t . Furthermore, requests from R_t which remained unassigned at t leave the system. New requests R_{t+1} enter the system between t and $t + 1$.

Policy: Let \mathcal{X} denote the set of possible AMoD system states. A (deterministic) policy $\delta : \mathcal{X} \rightarrow \mathcal{Y}$ is a mapping that assigns to any AMoD system state x a decision $y \in \mathcal{Y}(x)$.

Objective: Let us denote by $p_{v,t}$ the reward made by vehicle v at time t . The reward at time t is therefore

$$P_t = \sum_{v \in V} p_{v,t}. \tag{2.1}$$

We may adjust the objective by changing the interpretation of $p_{v,t}$; for example, we can maximize the total profit by accounting for trip-dependent rewards and costs. Alternatively, we can maximize the number of served requests by setting $p_{v,t}$ to the number of requests that vehicle v serves at

time t . Our objective is to find a policy δ that maximizes the total reward over all vehicle trips at the end of the problem time horizon T ,

$$\max_{\delta} \mathbb{E} \left(\sum_{t=1}^T P_t | \delta \right). \quad (2.2)$$

Full-information upper bound: We can compute a full-information upper bound by supposing that all requests $\bigcup_t R_t$ are already in the system at time $t = 1$.

Scope and limitations of the model: A few comments on this modeling approach are in order. First, we do not permit late arrivals at pick-up locations. When a request enters the system, the central controller decides to either fulfill or reject this request. This assumption aligns with real-world practice: customers typically can choose between various mobility providers such that an unfulfilled request usually leads to a customer choosing another provider’s service or resubmitting the request a bit later. Consequently, operators aim to take immediate action to provide direct feedback to customers. Notably, it is possible to adapt our setting for delayed pickups by including unfulfilled requests in the request batch that enters the system in the next system time period. Second, we assume that ride-pooling decisions occur at an upper planning stage. Analyzing whether a hierarchical or an integrated ride pooling approach is superior for CO-enriched ML online control of AMoD systems remains an open research question for future work. Third, we consider travel time uncertainty on a lower operational level. We can express time uncertainty on the duration of each ride request which has no impact on the presented model.

3. CO-enriched ML pipeline

Recall that a policy maps an AMoD system state to a feasible dispatching and rebalancing decision. Since the set of feasible dispatching and rebalancing decisions $\mathcal{V}(x)$ is composed of collections of disjoint trips, which can be represented as a collection of disjoint paths in a digraph with requests as vertices, it is tempting to model the problem of choosing a decision as a k -disjoint shortest paths problem (k -dSPP). Unfortunately, there is no natural way of defining the parameters of this problem. To mitigate this, we propose a learning pipeline illustrated in Figure 1 to encode our policies. It includes a k -dSPP as a combinatorial optimization layer that selects the decisions. This layer captures the combinatorial structure of the decisions and can be efficiently solved using polynomial algorithms.

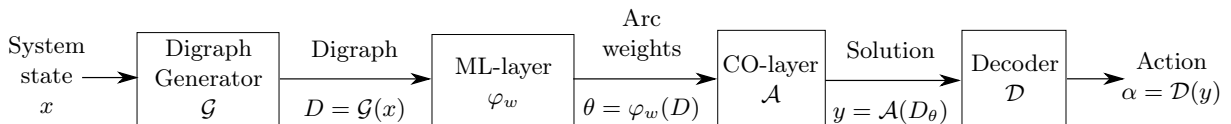


Figure 1: The hybrid CO-enriched ML pipeline.

Our pipeline is as follows. In general, the input to the hybrid CO-enriched ML pipeline is a system state x . In our specific application (cf. Section 2), we can interpret a system state x as an AMoD system state at time t , $x_t = (R_t, (x_{v,t})_{v \in V})$, which comprises the current ride request batch R_t and the vehicle states $x_{v,t}$ of all vehicles $v \in V$. The pipeline forwards this system state x to the digraph generator layer \mathcal{G} , which transforms the system state into a digraph D so that a path in the digraph D is a feasible vehicle trip. The second layer, the ML-layer, receives the digraph D and uses an ML-predictor φ_w to predict the respective arc weights θ of digraph D . Accordingly, the ML-layer returns a weighted digraph D_θ , which we refer to as the CO-layer-digraph. The third layer, the CO-layer, then consists of a k -dSP-algorithm \mathcal{A} that solves a k -dSPP on the weighted CO-layer-digraph D_θ and returns a solution y . Finally, a decoder \mathcal{D} transforms the vehicle trips y to a feasible dispatching and rebalancing action α .

The main rationale of this hybrid CO-enriched ML pipeline is to learn the weights θ of the CO-layer-digraph D_θ based on optimal full-information solutions so that the k -dSPP returns a good solution $y \in \mathcal{Y}(x)$.

In the remainder of this section, we show in Section 3.1 how the digraph generator layer \mathcal{G} generally models a dispatching problem as a digraph so that we can set its weights in the ML-layer and solve it with a k -dSPP in the CO-layer. We then detail two variants of the CO-enriched ML pipeline in Section 3.2, and Section 3.3 respectively. These two pipelines represent two different possibilities to enable rebalancing actions and only differ in their digraph generator layer \mathcal{G} . In Section 3.4, we finally derive the SL problem to learn an ML-predictor for these pipelines.

3.1. Dispatching Problem

In the following, we show how to formulate our dispatching and rebalancing problem as a k -dSPP, which yields the basis for the policies that we introduce in Section 3.2 and Section 3.3. Specifically, we define a dispatching graph as illustrated in Figure 2a. We construct our dispatching graph as a weighted and directed graph $D = (V, A, \theta)$ with a set of vertices V , a set of arcs A , and a vector of

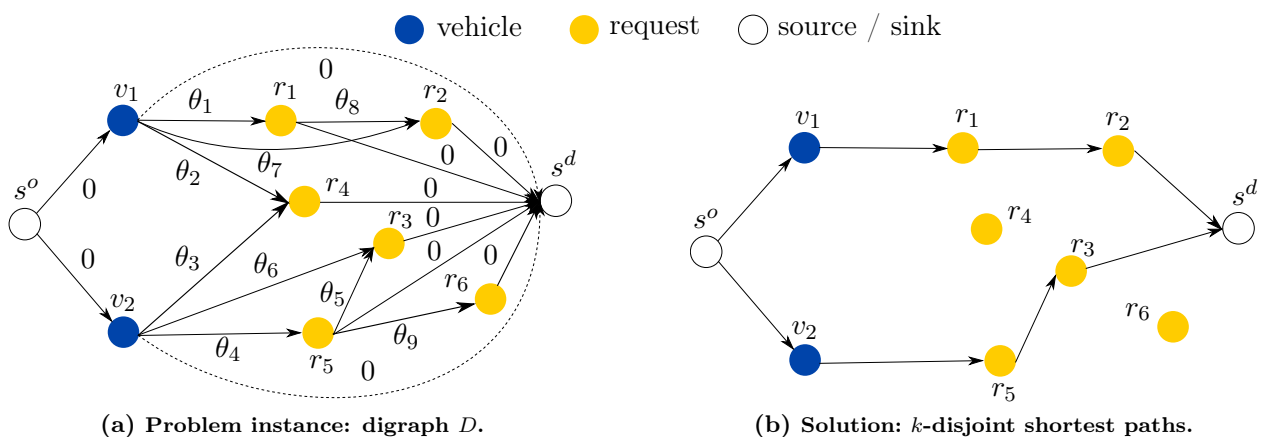


Figure 2: Example of the dispatching problem modeled as a digraph (a) and a corresponding solution (b).

weights θ , which comprises a weight θ_a for each arc $a \in A$. The vertex set $V = V^v \cup V^r \cup V^a \cup \{s^o, s^d\}$ consists of a subset of vehicle vertices V^v , a subset of request vertices V^r , a subset of artificial vertices V^a , a dummy source vertex s^o , and a dummy sink vertex s^d . Here, we associate each request vertex with a customer request, while we associate each vehicle vertex with a vehicle’s initial position at the beginning of the system time period or the location where the vehicle will end its previous trip. Furthermore, we associate each artificial vertex with a rebalancing action. For now, we assume the set of artificial vertices V^a to be empty to simplify the example in Figure 2. We then construct the arc set as follows: we create an arc between two request vertices if request-to-request connectivity is possible, i.e., Constraint (ii) in Section 2 holds. Moreover, we create an arc between a vehicle vertex and a request vertex if vehicle-to-request connectivity is possible, i.e., Constraint (iii) in Section 2 holds. Finally, we connect the dummy source vertex with each vehicle vertex, and connect all vehicle, request, and artificial vertices to the dummy sink.

Note that D is acyclic by construction. Then, a path in D that starts at the dummy source vertex and ends at the dummy sink vertex represents a feasible vehicle trip. This trip can unambiguously be associated with a certain vehicle as its second vertex is always a vehicle vertex. To finally devise our dispatching problem, we assign a weight θ_a to each arc $a \in A$. We set the weights of arcs that enter the sink or leave the source to zero. Additionally, we set the weights of arcs that enter a request vertex depending on the use case: in the CO-enriched ML pipeline our ML-predictor φ_θ predicts the weights.

In a full-information setting, we can set the weight of a request’s ingoing arc according to its negative reward $-p_r$. We can then find an optimal solution to the CO-layer problem that maximizes the total reward of the central controller by solving a k -dSPP on D_θ , with k being the number of vehicles of the AMoD fleet. Figure 2b illustrates an example of a resulting solution in which each disjoint path defines a trip sequence for a specific vehicle. The resulting solution is feasible as the disjointness of the paths ensures Constraint (i), while Constraints (ii)–(iii) are ensured due to the structure of D_θ . The complexity of solving a k -dSPP on D_θ is in $O(|A|(|V| + k) + k|V| \log |V|)$ (cf. Schiffer et al. 2021), such that we obtain a polynomial algorithm to solve the problem of dispatching vehicles to requests.

Three comments on this algorithm are in order. First, the resulting solution can contain empty trip sequences that indicate inactive vehicles if this benefits the overall reward maximization. In this case, some paths consist of a vehicle vertex being directly connected to the source and sink vertex. Second, one may change the objective of the central controller by modifying the graph’s weights, e.g., to maximize the profit of the central controller, we correct a request’s reward with arising costs for fulfilling this request. Third, one may further speed up the resulting algorithm by deleting connections of D to receive a sparse graph, e.g., by connecting only request vertices for which the associated requests are within a certain vicinity. We discuss such a sparsification heuristic in Appendix D.

3.2. Sample-Based (SB) Pipeline

We recall that the main rationale of the hybrid CO-enriched ML pipeline is to use an ML-predictor to predict the weights of the CO-layer digraph, such that solving the k -dSPP yields an anticipative dispatching and rebalancing solution. A major drawback of the so far presented CO-layer digraph D_θ is that it only considers vehicle states $x_{v,t}$ for all $v \in V$ and the current request batch R_t to take a dispatching action in system time period $[t, t + 1)$. Accordingly, decisions based on this policy are rebalancing-agnostic, and do not consider future ride requests or any possibility to incorporate rebalancing actions. The SB pipeline addresses both of these drawbacks by sampling future ride requests and incorporating them into our digraph. In the following, we detail the components of the SB pipeline.

Digraph Generator: To extend the digraph, we first extend a system state by enlarging its system time period $[t, t + 1)$ with a prediction horizon $[t + 1, t^{\text{pred}})$. Then, the system time period and the prediction horizon form an extended horizon for which we predict a set of artificial requests. To extend the digraph D , we create an artificial vertex $r \in V^a$ with $s_r \in [t + 1, t^{\text{pred}})$ for each artificial request, and enlarge the arc set accordingly to obtain an extended digraph, see Figure 3.

In this paper, we predict artificial requests by sampling from a request distribution calibrated on historical data, which has proven to yield state-of-the-art results within related online algorithms (cf. Alonso-Mora et al. 2017). To do so, we partition the fleet’s operating area into a rectangular grid, divided into equally-sized squares, and refer to each square as a rebalancing cell. Each rebalancing cell comprises its own request distribution. We note that one can easily replace this sampling with a more sophisticated predictor. In this case, one could even avoid the usage of rebalancing cells. However, as the size of these cells is usually rather small, the resulting accuracy increase remains limited.

ML-layer: Given all the information available, we predict the weight θ_a for each arc of the digraph using a generalized linear model, $\theta_a = \langle w | \phi(a, x) \rangle$, where $\phi(a, x)$ is a features vector, which depends

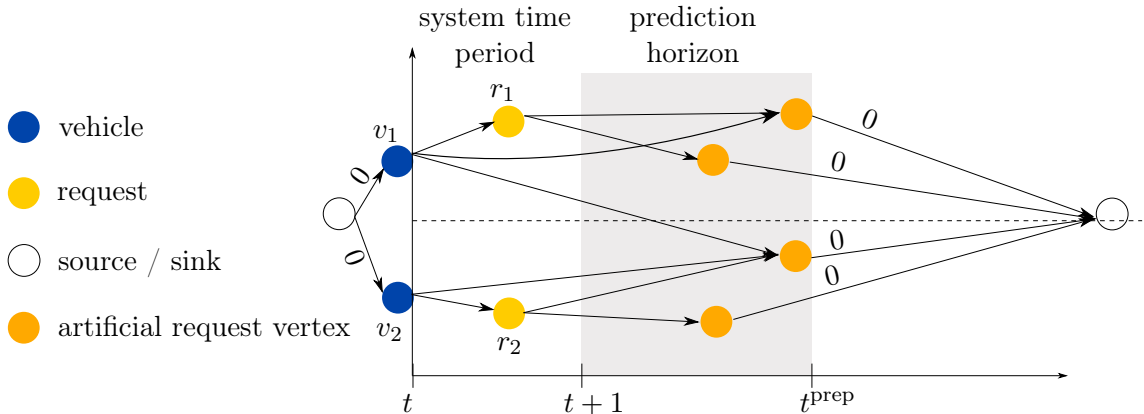


Figure 3: Example of an extended digraph with predicted requests in the prediction horizon $[t+1, t^{\text{prep}})$.

on arc a and system state x . Here, the system state x can also incorporate historical information. Note that we detail the features used in Appendix C. Intuitively, a weight on an artificial request’s ingoing arc represents the learned reward of rebalancing to the location of the artificial request.

CO-layer: The CO-layer solves the k -dSPP on the CO-layer-digraph D_θ .

Decoder: The decoder \mathcal{D} receives k disjoint paths, each representing a vehicle trip, and returns a dispatching and rebalancing action for each vehicle. When a vehicle path goes through r , we dispatch the vehicle to r if r is an actual request, i.e., $s_r \in [t, t + 1)$, and we rebalance the vehicle to the location of r if r is an artificial request, i.e., $s_r \in [t + 1, t^{\text{pred}})$. We refer to the resulting SB policy with δ_{SB} .

A major drawback of the SB policy presented in Section 3.2, and state-of-the-art benchmarks (see, e.g., Alonso-Mora et al. 2017), is the need for additional distributional information on future ride requests. To omit the need for this distributional information, we propose a CB pipeline, which aims to extend the digraph with capacity vertices in each rebalancing cell such that it is possible to learn distributional information when learning the weights of the digraph. In the following, we detail the components of the CB pipeline.

3.3. Cell-Based (CB) Pipeline

Digraph Generator: We partition the fleet’s operating area into a rectangular grid, divided into equally-sized rebalancing cells. We add one rebalancing action as an artificial rebalancing vertex $r \in V^a$ for each rebalancing cell and connect it to a set of artificial capacity vertices from V^a as shown in Figure 4. We refer to the digraph with artificial vertices as the extended digraph.

ML-layer: Again, we predict the weights θ_a using a generalized linear model $\theta_a = \langle w | \phi(a, x) \rangle$. The weight θ_a of each rebalancing vertex’s ingoing arc reflects the reward of a relocation to the

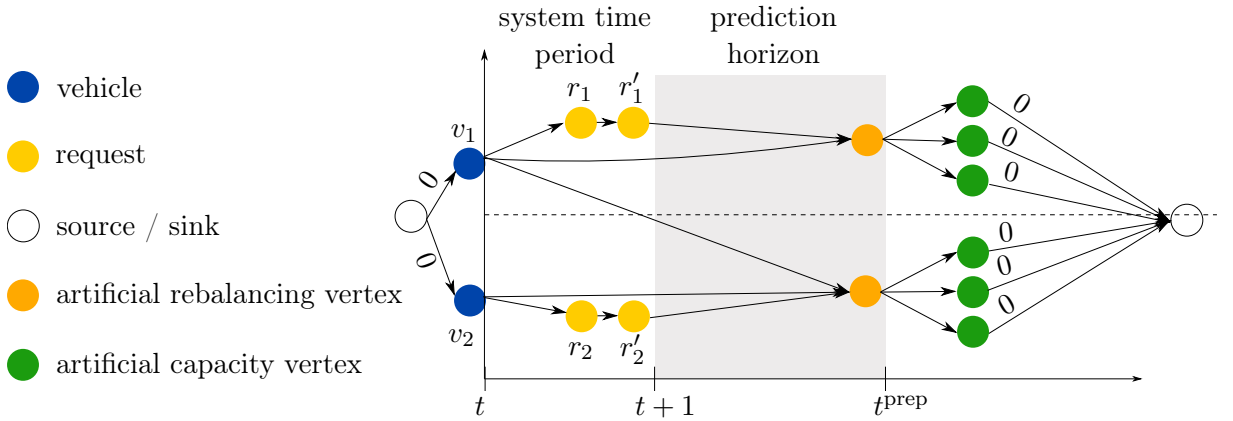


Figure 4: Extended digraph with rebalancing vertices in prediction horizon $[t + 1, t^{\text{pred}})$ and capacity vertices.

respective rebalancing cell, and the weight of each capacity vertex’s ingoing arc reflects the reward of each additional vehicle rebalancing to this cell.

CO-layer: Following this pipeline requires us to rethink our k -dSPP approach as we face the following conflict: in the created graph structure, multiple paths need to share a rebalancing vertex to learn the value of multiple rebalancing actions to the same location correctly. On the other hand, we still require paths to be vertex-disjoint with respect to request vertices to ensure dedicated request-to-vehicle assignments. To resolve this contradiction, we adapt the k -dSPP from finding vertex-disjoint paths to finding arc-disjoint paths, which allows paths to share a rebalancing vertex. To ensure disjoint request vertices between paths, we then split each request vertex into two vertices and introduce an arc with weight 0 to connect both vertices. Then we can solve an arc-disjoint k -dSPP on the CO-layer-digraph. The resulting paths may share rebalancing vertices but are disjoint with respect to request and capacity vertices.

Decoder: The decoder \mathcal{D} receives k disjoint paths and returns a dispatching and rebalancing action for each vehicle. When a vehicle path goes through r , we dispatch the vehicle to r if r is an actual request, i.e., $s_r \in [t, t + 1)$, and we rebalance the vehicle to the location of r if r is an artificial rebalancing vertex. The advantage of the CB pipeline is that it embeds distributional information within the weights of the CO-layer-digraph and does not require any distributional information about future ride requests. We refer to this CB policy with δ_{CB} .

3.4. Structured Learning methodology

The policies resulting from the pipelines introduced in Sections 3.2 and 3.3 are clearly sensitive to the weights of the CO-layer-digraph D_θ . To effectively learn these weights θ , we leverage SL, i.e., we aim at learning θ in a supervised fashion from past full-information solutions. To do so, we must derive a direct relation between the weights θ and the resulting policy decisions encoded via solution paths y . Therefore, we introduce the following notation: we denote a CO-layer-digraph as x_i and embed the set of all feasible solutions $\mathcal{Y}(x_i)$ in $\mathbb{R}^{|A|}$ so that $y \in \mathcal{Y}(x_i)$ is a vector $(y_a)_{a \in A}$ with

$$y_a = \begin{cases} 1, & \text{if arc } a \text{ is in } k\text{-disjoint solution paths} \\ 0, & \text{otherwise.} \end{cases} \quad (3.1)$$

Then, we can formulate the CO-layer-problem, namely the k -dSPP, as a maximization problem

$$\hat{y}_i(\theta) = \arg \max_{y \in \mathcal{Y}(x_i)} \theta^T y. \quad (3.2)$$

Here, our goal is to find a θ such that $\hat{y}_i(\theta)$ leads to an efficient policy for all x_i at our disposal. To do so, we use a learning-by-imitation approach. Practically, we build a training set $(x_1, y_1^*), \dots, (x_n, y_n^*)$ containing n instances x_i of the CO-layer problem (3.2) as well as their solution y_i^* that we want to

imitate. We then formulate the learning problem as,

$$\min_{\theta} \frac{1}{n} \sum_{i=1}^n L(\theta, x_i, y_i^*), \quad (3.3)$$

where the loss function $L(\theta, x, y^*)$ quantifies the non-optimality when using $\hat{y}(\theta)$ instead of y^* . In the following, we explain how we build $\{(x_1, y_1^*), \dots, (x_n, y_n^*)\}$, which loss L we use, and how to solve (3.3).

Building the training set:

We aim to imitate an optimal full-information bound, which cannot be derived during online decision-making because it requires information about future requests. Accordingly, we build a training set from historical data, which allows us to generate a training set based on full-information solutions. Our training set contains a training instance (x_i, y_i^*) for each system time period of every problem instance at our disposal. We generate y_i^* as follows: we solve the full-information problem of the respective historical problem instance for the complete problem time horizon. To do so, we modify the CO-enriched ML pipeline. In the digraph generator layer, we generate a digraph with all requests of this full-information problem. In the ML-layer, we set the weights of a request's ingoing arc according to the reward which the central controller receives for fulfilling the respective request. Subsequently, we solve the CO-layer-problem (3.2) which retrieves the full-information solution. From this full-information solution, we rebuild the digraph x_i of Problem (3.2) for the system time period of interest (see Figure 5a) and assign the corresponding full-information solution y_i^* to it (see Figure 5b).

Fenchel-Young loss:

Given a training point (x_i, y_i^*) , we want to find a θ such that the solution of problem (3.2), namely $\hat{y}_i(\theta)$ equals the optimal solution y_i^* . It is therefore natural to use as

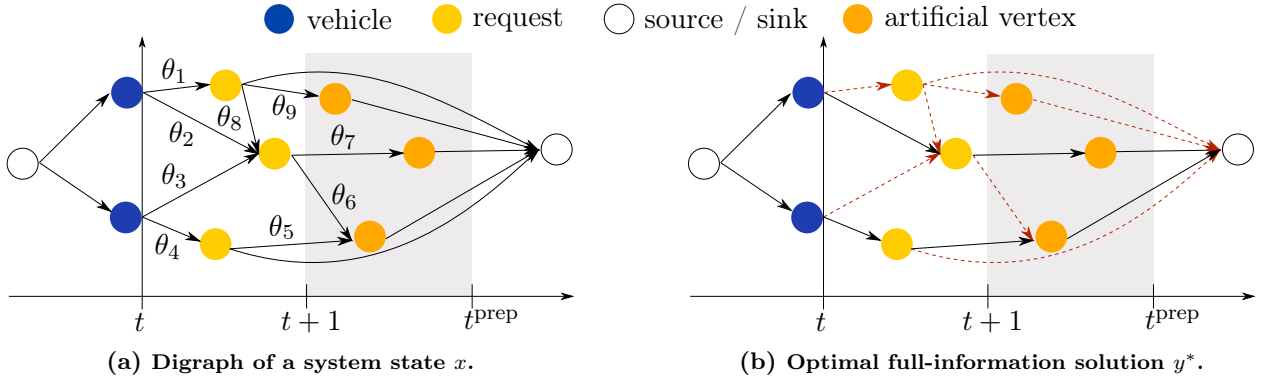


Figure 5: Example digraph (left) and the corresponding optimal full-information solution (right). The solid black paths in the optimal full-information solution represent the dispatching solution as k -disjoint shortest paths. The SL approach learns the weights of the digraph such that the solution coincides with the solid black path of the optimal full-information solution.

loss $L(\theta, x_i, y_i^*)$ the non-optimality of $\hat{y}_i(\theta) = \arg \max_{y \in \mathcal{Y}(x_i)} \theta^T y$ as a full-information solution

$$L(\theta, x_i, y_i^*) = \underbrace{\max_{y \in \mathcal{Y}(x_i)} (\theta^T y) - \theta^T y_i^*}_{\text{non-optimality of } \hat{y}_i \text{ as a full-information solution}}, \quad (3.4)$$

i.e., we minimize the difference between the solution y induced by θ and the full-information solution y_i^* . Figure 5 visualizes the intuition of this loss function: the loss function minimizes the difference between the sum of weights from the CO-layer solution (left side of (3.4) and Figure 5a) and the sum of weights from the full-information solution (right side of (3.4) and Figure 5b). When minimizing loss function (3.4), we aim to adapt the weights θ such that the CO-layer solution coincides with the full-information solution.

Unfortunately, the learning problem (3.3) combined with loss (3.4) contains a trivial solution with $\theta = 0$. In this case, any feasible solution from \mathcal{Y} is an optimal solution of the CO-layer-problem (3.2), which results in a random policy. We follow Berthet et al. (2020) and fix this issue by adding a Gaussian perturbation Z to θ , which has a regularizing effect,

$$L(\theta, x_i, y_i^*) = \underbrace{\mathbb{E} \left[\max_{y \in \mathcal{Y}(x_i)} (\theta + Z)^T y \right] - \theta^T y_i^*}_{\text{non-optimality of } \hat{y}_i \text{ as a solution of the perturbed CO-layer problem}}. \quad (3.5)$$

Solving the learning problem: An analysis based on Fenchel-Young convex duality enables us to show that this loss is smooth and convex (cf. Berthet et al. 2020) with the following gradient

$$\nabla_{\theta} L(\theta, x_i, y_i^*) := \mathbb{E} \left[\arg \max_{y \in \mathcal{Y}(x_i)} (\theta + Z)^T y \right] - y_i^*. \quad (3.6)$$

For further discussion of smoothness and convexity properties and the gradient derivation, we refer to Appendix A.

Considering this gradient, we can minimize the learning problem (3.3), with loss (3.5) with respect to θ . As θ is a prediction of the ML-predictor φ_w , we need to backpropagate the gradient through φ_w to learn w . To do so, the predictor φ_w must be differentiable. A straightforward differentiable predictor is a linear model

$$\theta_a = \langle w | \phi(a, x_i) \rangle \quad \forall a \in A, \quad (3.7)$$

and with this linear model, $w \mapsto L(\varphi_w(x_i), x_i, y_i^*)$ remains convex. Although we have now defined all items in (3.5) and (3.6), we can still neither calculate the loss nor its gradient as computing the expectation remains intractable. Therefore, we use a sample average approximation of (3.6) to calculate a gradient. With this gradient, we can then minimize a sample average approximation of (3.5) with a Broyden–Fletcher–Goldfarb–Shanno (BFGS) algorithm. The BFGS is a quasi-Newton algorithm that performed well on such problems (cf. Parmentier 2021, Parmentier & T’Kindt 2022).

4. Experimental Design

This section details our experimental design by first introducing our real-world case study in Section 4.1 and afterward detailing our benchmark policies in Section 4.2.

4.1. Case Study

Our case study focuses on an online AMoD control problem for the New York City Taxi data set (NYC Taxi & Limousine Commission 2015) from the year 2015. We chose the year 2015 as it is the most recent year with exact recordings of starting and destination locations from ride requests, and restrict the simulation area to Manhattan. We model vehicle movements with exact longitude and latitude values. To avoid a computational overload for on-the-fly computation of driving times, we use a look-up table to retrieve the distance and the time needed to drive from a starting location to a destination location. We base this look-up table on data from Uber Movement for the year 2020 (Data retrieved from Uber Movement, (c) 2022 Uber Technologies, Inc., <https://movement.uber.com.>), which accounts for traffic conditions accordingly. Each location in this look-up table is specified by a rather small square cell of size 200 meters \times 200 meters. If the starting and destination locations are in the same cell, we assume a line distance and an average driving speed of 20 kilometers per hour. The rebalancing cells are specified by larger square cells of size 333 meters \times 333 meters to represent rebalancing areas.

We only consider weekdays as we assume different travel behavior on weekends, and focus on an AMoD system operating for one hour from 9 AM till 10 AM. We assume a system time period of one minute such that the central controller can apply dispatching and rebalancing actions every minute. We split data into disjoint sets of training data, validation data, and testing data. The training data and the validation data comprise 5 working days \times 1 hour of request data, and the testing data comprises 20 working days \times 1 hour of request data. We stop the training after 70 training iterations or a maximum of 70 hours of training time. When discussing results, we report the averaged results over the testing data.

To further speed up the computation times of our k -dSPP algorithm, we apply sparsification techniques to sparsify the CO-layer-digraph. For a detailed description of this sparsification, we refer to Appendix D. For our specific case study, we finally only include an arc in the CO-layer-digraph if the distance to the next request is below 1.5 kilometers, and if the next request is reachable within 720.0 seconds. These thresholds permit to significantly sparsen our digraph but have hardly any effect on the solution quality. Note that these thresholds are problem and instance specific and should be recalibrated for other use cases.

We generate different scenarios with varying fleet sizes ranging from 500 to 5000 vehicles, and scenarios with different ride request densities, ranging from 10% to 100% of the original ride request volume. In each scenario, we optimize over profit and the number of satisfied customers. When we optimize over profit, we take the revenue for fulfilling the request extracted from (NYC Taxi & Limousine Commission 2015) minus operational costs of 0.45\$ per driven kilometer (Bösch et al. 2018).

When we optimize over the number of satisfied customers, we take a revenue of 1 for fulfilling a ride request minus marginal costs of 0.00001 per driven kilometer, to retrieve a lexicographic objective that maximizes the number of satisfied ride requests but prefers sustainable solutions with fewer kilometers driven over less sustainable solutions. If not specified differently, we assume a base scenario that considers 30% of the original ride request volume and a vehicle fleet size of 2000 vehicles. Here, we chose a request share of 30% to reflect a typical market share of a ride-hailing fleet (cf. Statista 2021). We then set the vehicle fleet size such that it enables a 100% request fulfillment under an optimal full-information approach.

Discussion A few comments on the setup of this case study are in order. First, we decided to evaluate the system on a one-hour period for several reasons: Learning a policy that operates longer than a one-hour period requires solving an offline dispatching problem which is computationally hard for large-scale scenarios. However, operating the system longer than a one-hour period is easily possible by operating individually trained policies in each hour. As the performance of our algorithms is similar over different hours of a day, we only report this one-hour period for better comparison. Second, we experience that our CO-enriched ML pipeline leads to very general policies, shown by superior average performance over weekdays, although the request distribution might change from Monday to Friday. In this context, one may argue that demand patterns can change more drastically between different seasons e.g., from winter to summer, or weekday to weekend. For such cases, our analyses are still valid as one can easily either train separate models for drastically different scenarios or add context to the predictor to enhance its generalizability further. Third, we limit our studies to one case study and train our model for this respective case. This is common practice, as generalizing across different case studies can be an unnecessary tedious task. In practice as well as in research there is some consensus that applying a learning-based model to a different ground truth is better handled by retraining, which is also the case for our model: to apply our pipeline to a different city, it needs to be retrained.

4.2. Benchmark policies

In our computational studies, we apply the following benchmark policies.

Greedy Policy: The greedy benchmark policy is an online policy that greedily re-optimizes dispatching decisions in a rolling horizon fashion. The greedy policy does not include any rebalancing vertices into the digraph and, instead of learning the weights of arcs in the digraph, sets the weight of a request’s ingoing arc according to its reward. Solving a k -dSPP on this digraph leads to greedy dispatching actions which only incorporate requests that are within the actual system time period.

Sampling Policy: The sampling benchmark policy is an online policy that re-optimizes dispatching and rebalancing decisions in a rolling horizon fashion and samples future requests for the prediction horizon from historical data. We can interpret the sampling policy also as a vari-

ant of an CO-enriched ML pipeline with a digraph generator that incorporates sampled ride requests as artificial rebalancing vertices in the digraph. Instead of learning the weights of arcs in the digraph, it sets the weight of a request’s ingoing arc according to its reward. To prefer real requests from the system time period over sampled requests from the prediction horizon, we multiply the reward of sampled ride requests with a discount factor of 0.2 as we received the best results for this factor. We consider a prediction horizon of four minutes as it leads to best results (see Appendix E).

Full-information bound (FI): We compute a full-information bound with complete information about all ride requests. Solving the full-information problem optimally constitutes an upper bound for the online problem. To compute the full-information solution, we assume a system time period equal to the problem time horizon $[1, T)$, such that all ride requests $\bigcup_t R_t$ are available at the system at time $t = 1$. Accordingly, the digraph at $t = 1$ comprises all requests of the complete problem time horizon. Therefore, we do not have to predict the arc weights in the digraph but can set the arc weights of an arc equal to the reward for the ingoing request vertex.

Sample-Based (SB) Policy: The SB policy is an online policy that follows the variant of the CO-enriched ML pipeline presented in Section 3.2. The policy re-optimizes dispatching and rebalancing actions in a rolling horizon fashion. For the SB policy, we consider a prediction horizon of four minutes, as we received the best results for this planning horizon (see Appendix F).

Cell-Based (CB) Policy: The CB policy is an online policy that follows the variant of the CO-enriched ML pipeline presented in Section 3.3. The policy re-optimizes dispatching and rebalancing actions in a rolling horizon fashion. We set the number of capacity vertices for every rebalancing cell to one, as we achieved the best results with this setting. For the CB policy, we consider a prediction horizon of four minutes, as we received the best results for this planning horizon (see Appendix F).

One comment on the selection of our benchmark policies is in order. One may wonder why we do not explicitly consider any DRL-based policy. In fact, all publications that present a DRL-based policy benchmark this policy solely against a greedy baseline algorithm. Accordingly, by benchmarking our learning-based policies against the greedy benchmark suffices to discuss the performance of our policies against DRL-based approaches and keeps the results section as concise as possible.

5. Results

In the following, we first present the results of the real-world case study for different vehicle fleet sizes and request densities in Section 5.1. We then provide an in-depth structural analysis for the SB and CB policies and compare them with the other benchmark policies with respect to external effects and computational time in Section 5.2.

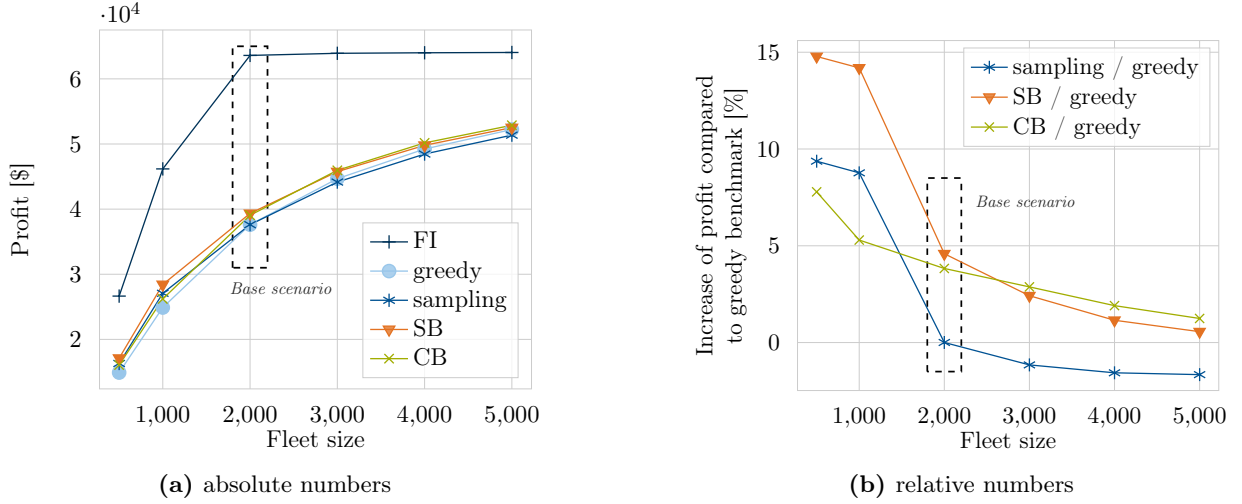


Figure 6: Scenarios with different fleet sizes when optimizing the profit.

5.1. Performance Analysis

To analyze the performance of our learning-based policies, we benchmark their performance for various scenarios with varying fleet sizes and request densities as well as for varying objectives, first focusing on profit maximization.

Varying fleet size: Figure 6 shows the performance of the SB policy and the CB policy compared to the greedy and sampling policy, and to the full-information bound for different fleet sizes when maximizing the profit. Here, the data point with a fleet size of 2000 vehicles constitutes our base scenario. As can be seen, there is a significant gap between the full-information bound, which remains an upper bound, and all other policies, see Figure 6a. This gap reduces for increasing or decreasing fleet sizes as in the former case, the assignment of requests to vehicles gets less error sensitive, while in the latter case, the objective value of the full-information solution decreases overproportionally due to the reduced solution space.

To ease the comparison between all online policies, Figure 6b compares both the SB and the CB policy as well as the sampling policy against the greedy policy. In the base scenario, both the SB and the CB policy outperform the greedy and the sampling policy: while the SB policy improves upon the greedy policy by 4.6%, the CB policy improves upon the greedy policy by 3.8%, and the sampling policy matches the performance of the greedy policy. For increasing fleet sizes, the performance difference between the SB and CB policies decreases. Remarkably, the sampling policy performs even worse than greedy in these cases. For decreasing fleet sizes, all policies show an increased performance gain compared to the greedy policy as the anticipation and prioritization of profitable requests is even more crucial in this setting. Here, the SB policy still outperforms all other policies but the sampling policy shows a larger improvement compared to the CB policy. These results indicate that the CO-enriched ML pipeline outperforms state-of-the-art matching and rebalancing algorithms, e.g., the sampling benchmark which is similar to the model predictive control approach

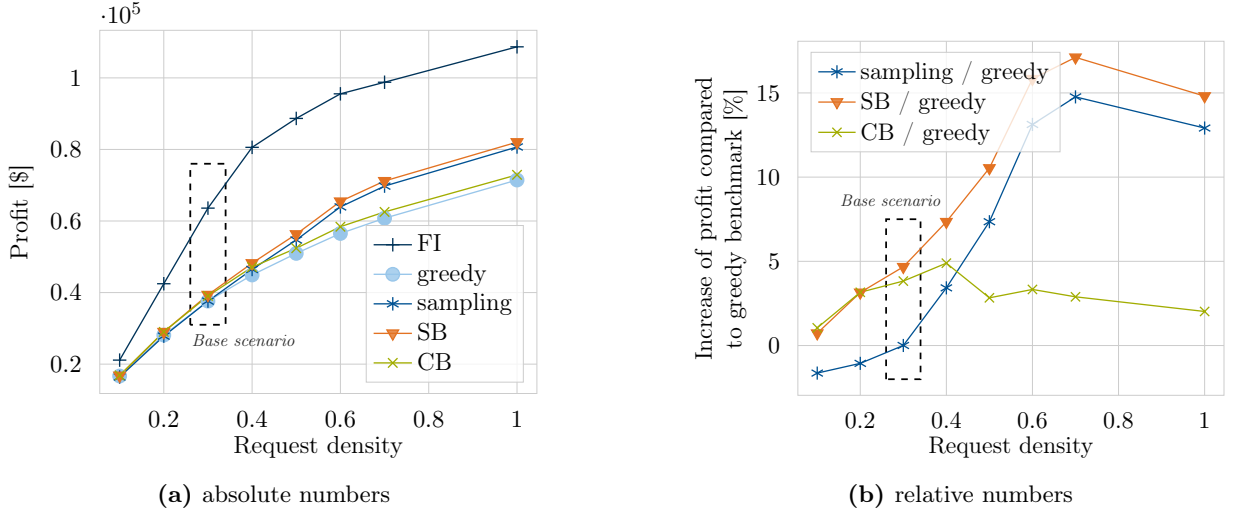


Figure 7: Scenarios with different request densities when optimizing the profit.

of Alonso-Mora et al. (2017), as well as state-of-the-art DRL algorithms which only outperform greedy policies by around 2-5% (cf. Enders et al. 2023).

Result 1. *Both the SB and CB policies robustly improve over the greedy policy, while the sampling policy shows a fragile performance, often performing worse than the greedy policy. The SB policy outperforms all other policies with improvements over the greedy policy of up to 14.8%. The CB policy outperforms the sampling policy in most scenarios although the CB policy does not require distributional information on future ride requests.*

Varying request density: Figure 7 extends our performance analysis by showing the performance of all different policies for different request densities when fixing the number of vehicles to 2000. For scenarios with a higher request density than in our base scenario, the SB policy outperforms all other online policies with average improvements of 13.1% compared to a greedy policy. The sampling policy shows average improvements of 10.3% for increasing request densities. For decreasing request densities, the sampling policy performs even worse than the greedy policy.

Unsurprisingly, the sampling policy does not perform as well on low request densities as it does on high request densities. Indeed, it relies on a single sampled scenario to take decisions. When there are very few requests, a single scenario can be seen as mostly noise and does not provide accurate information on the distribution of requests. Addressing this issue with a sampling-based approach would require sampling several scenarios, which would lead to a two-stage stochastic formulation. Such a formulation would make the policy much more computationally intensive, and difficult to apply in practice. On the contrary, our CB and SB policies robustly perform better than greedy, also for low request densities. This holds even for the SB policy although it inherits the same weakness as the sampling policy as it samples rebalancing locations. This shows the robustness of our learning-based policies compared to the sampling policy, and further indicates their superiority in terms of solution quality.

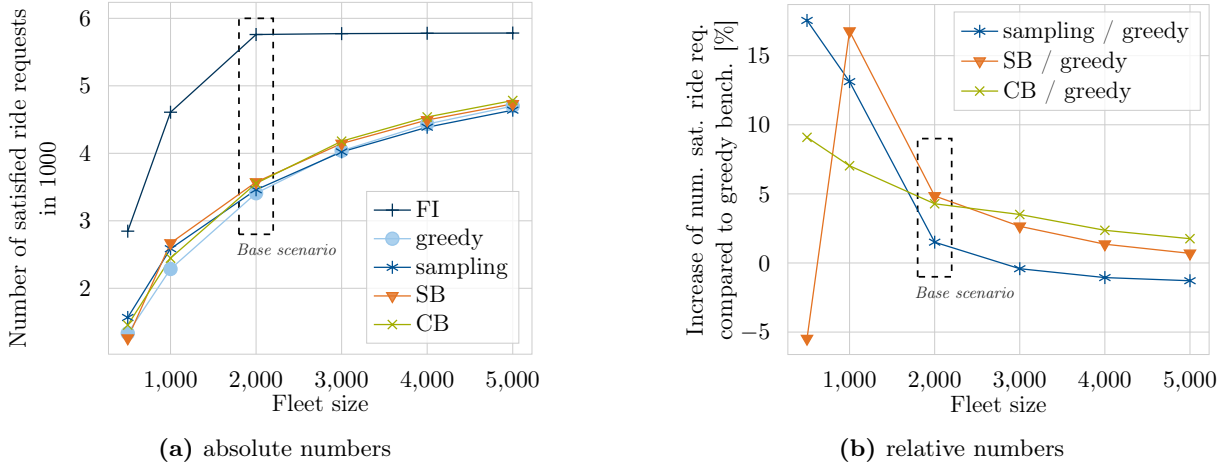


Figure 8: Scenarios with different vehicle fleet sizes when optimizing the number of satisfied customers.

Result 2. *The CB and SB policies yield a stable performance and improve upon greedy across all request densities. Contrarily, the sampling policy performs well on high request densities but badly on low request densities.*

Maximizing number of satisfied customers: Figure 8 extends our analysis to a different objective and shows the performance of all policies for a varying fleet size when maximizing the number of satisfied ride requests. As can be seen, our SB policy outperforms all other policies, improving by up to 16.8% compared to a greedy policy for fleet sizes between 1000 and 5000 vehicles. Again, we observe that the difference between a greedy policy and our learning-based policies decreases for increasing fleet sizes, while the sampling policy performs even worse than a greedy policy in such cases. However, we also observe one outlier: while our SB policy performs worse than the greedy policy in the artificial case of 500 vehicles, the sampling policy outperforms the greedy policy in this case. This is due to the fact that in this case, the request-to-vehicle ratio is very large such that the pure information about possibly available requests, which we obtain by sampling, suffices to achieve a good algorithmic performance. This is particularly possible since any request—independent of its duration or cost—adds the same contribution to the objective when solely maximizing the number of satisfied requests. Note that we observe a completely opposite behavior as soon as we change the objective towards a request-sensitive target when optimizing the total profit (cf. Figure 6b): in this case, the SB policy yields an improvement of 14.8% compared to a greedy policy as the learning allows to estimate the value of potential future requests.

Result 3. *Our SB policy outperforms all other online policies across different objectives and various scenarios that reflect real-world applications. Our CB policy yields lower improvements than our SB policy, but shows a more robust performance for artificial corner cases.*

Conclusion: Our results show that our learning-based policies outperform a greedy and a sampling policy across varying objectives and scenarios with different fleet sizes and request densities.

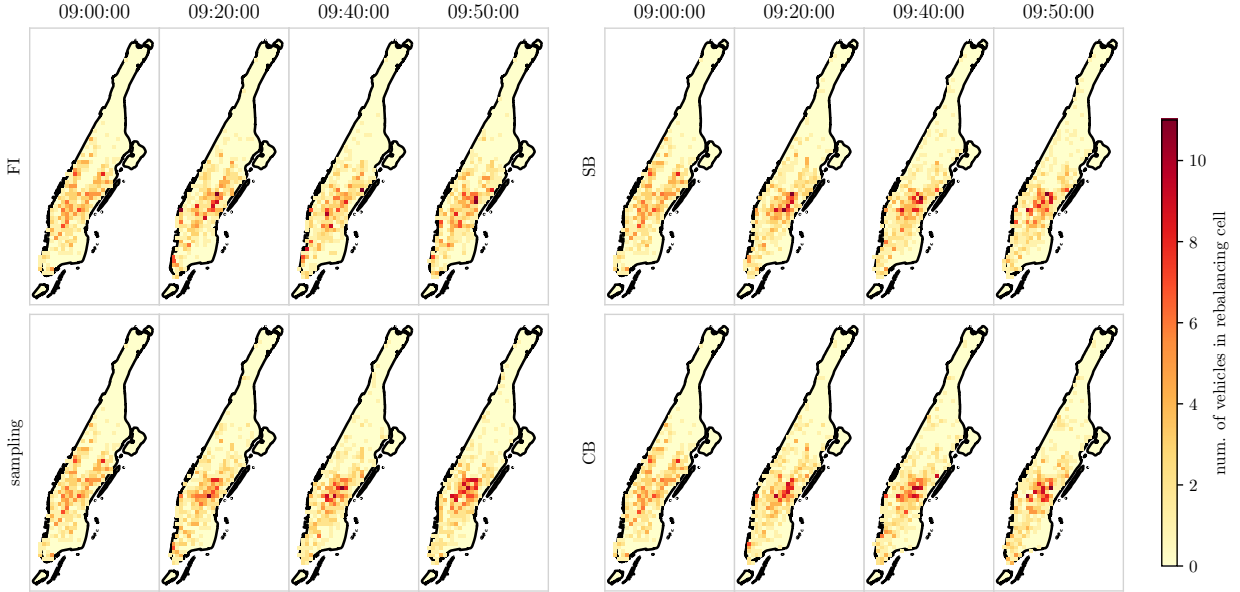


Figure 9: Vehicle distribution for different benchmark policies over different points in time for a representative instance.

In particular, our SB policy yields improvements up to 17.1% compared to a greedy policy for scenarios that reflect real-world applications. In these cases, our CB policy improves upon a greedy policy up to 9.1%, while a sampling policy shows an unstable performance that sometimes yields improvements, but oftentimes performs even worse than a greedy policy. In artificial corner cases, our SB policy may also perform worse than a greedy policy as it by design inherits some of the structural difficulties of any sampling-based approach. Here, our CB policy still shows a robust performance that improves upon a greedy policy.

5.2. Extended analysis

In the following, we deepen our analyses of the differences between the proposed benchmark policies. To this end, we analyze structural differences between the different policies and discuss their impact on external effects, as well as their efficiency with respect to computational times.

Structural Policy Properties: Figure 9 shows the evolution of the vehicle distribution for a representative instance over different points in time for the different benchmark policies. We interpret this evolution of vehicle distributions as an indicator of how the respective benchmark policies differ in their dispatching and rebalancing behavior, and refer to our git repository (<https://github.com/tumBAIS/ML-CO-pipeline-AMoD-control>) for an interactive visualization of idling, dispatching, and rebalancing characteristics of all policies. Compared to the full-information bound, the sampling policy leads to a compressed vehicle distribution in the city center, which occurs due to a biased rebalancing behavior that overvalues high-request-density areas over low-request-density areas. This leads to a significant amount of vehicles idling in high-request-density areas, which

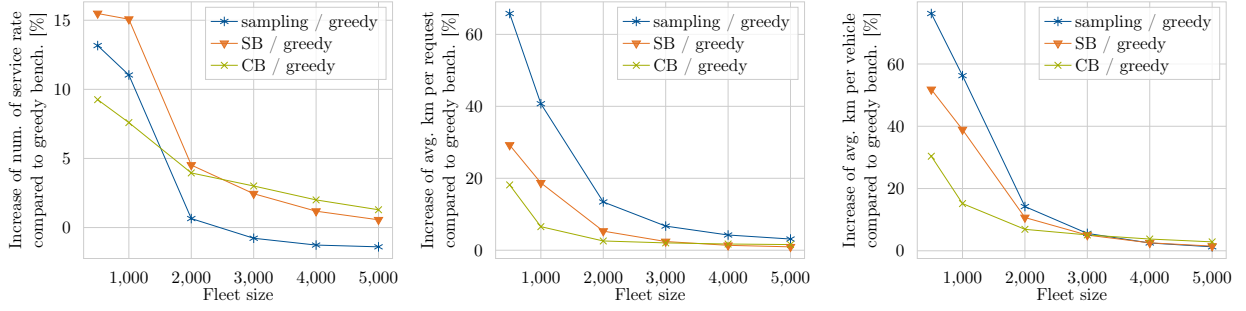


Figure 10: Externalities for all online policies compared to a greedy policy over various fleet sizes when optimizing the total profit.

leads to missed requests in mid to low-density areas and worsens the policy’s performance. The SB policy also shows a vehicle distribution that revolves around the city center and its high-request-density areas, which results from the fact that both policies leverage the identical historical request distribution for sampling future ride requests. However, the SL element allows anticipating better the value of relocations, which leads to vehicle distributions that still revolve around high-request-density areas but distribute a significantly larger share of vehicles to mid and low-density areas, which yields the performance improvement of our SB policy. The CB policy leads to a slightly more uniform vehicle distribution over the operating area as, by design, it restricts the maximum number of vehicles rebalancing to a rebalancing cell via the number of capacity vertices in each rebalancing cell. With these rebalancing actions, the CB policy yields a performance that is always better than greedy but remains below the performance of the SB policy.

Result 4. *While sample-based policies tend to rebalance too many vehicles to high-request-density areas, CB policies lead to a slightly more distributed rebalancing.*

Externalities: Figure 10 shows the externalities of our online policies compared to a greedy policy for different fleet sizes when optimizing the total profit. Here, we particularly focus on the number of served requests, the average number of kilometers driven per request, and the average number of kilometers driven per vehicle. As can be seen, the increase in the number of served requests is proportional to the profit increase for each policy. Accordingly, the SB policy yields the highest improvement for the number of served customers, and thus contributes to increase customer satisfaction. Remarkably, the SB policy yields a lower increase of average kilometers per request and per vehicle than the sampling policy, while at the same time yielding a higher number of passengers served and a higher profit. This highlights the efficacy of the SB policy, even for key performance indicators that are anticorrelated. We note that the SB policy still yields higher average kilometers driven per request and vehicle than the CB and greedy policies for small fleet sizes. This is due to the fact that these policies show a significantly lower performance on the anticorrelated key performance indicators, such as the number of satisfied requests and the total profit. For scenarios with large fleet sizes, when the SB and CB policies lead to a similar performance with regard to total profit, also the KPIs for average kilometers driven per request and vehicle are similar.

	Fleet size					
	500	1000	2000	3000	4000	5000
FI	2.314	4.396	10.155	14.949	27.59	28.792
greedy	0.012	0.05	0.208	0.485	0.863	1.384
sampling	0.041	0.169	0.588	1.201	2.003	3.01
SB	0.069	0.179	0.576	1.186	2.025	3.038
CB	0.093	0.312	0.905	1.798	2.966	4.167

Table 1: Average computational time to calculate dispatching and rebalancing actions [sec].

Result 5. *The SB policy yields a good trade-off between anticorrelated key performance indicators and outperforms the sampling policy on both the number of satisfied customers and the total profit as well as on the distance driven per request and vehicle.*

Computational time: Table 1 presents the average computational time to compute dispatching and rebalancing actions for all benchmark policies. We consider a system time period of one minute for all online policies and do not incorporate the time to construct the digraph. As can be seen, all policies benefit from the polynomial algorithm introduced in Section 3.1. While the greedy policy shows lower computational times compared to the sampling and learning-based policies, all online policies show computational times below a few seconds, which allow for application in practice when operating an AMoD system with a one-minute system time period.

Deep learning ML-layer: In the previous results, we used a linear predictor in the ML-layer to predict the digraph weights θ , according to equation (3.7). Instead of using a linear predictor, we can also use a differentiable deep learning predictor of the general form $\varphi_w : \phi(a, x_i) \rightarrow \theta_a \quad \forall a \in A$. For learning a deep learning predictor, some adaptations are in order in comparison to learning a linear predictor. First, instead of using the BFGS method, we use a stochastic gradient descent (SGD) method to optimize the learning problem (3.3). Second, the SGD method updates the weights w for each training instance instead of updating the weights with a mean gradient over all training

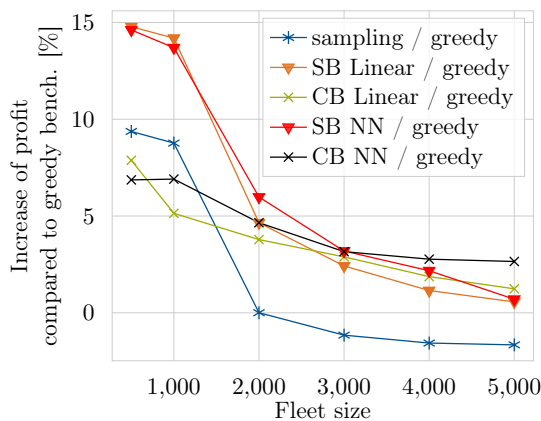


Figure 11: Comparison of performance with linear predictor and feedforward neural network (FNN) predictor.

instances. Third, for deriving a subgradient (3.6) we add a perturbation Z to θ instead of perturbing the weights w .

Figure 11 shows the performances of the CO-enriched ML pipeline for different vehicle fleet sizes when using an feedforward neural network (FNN) predictor, and a linear predictor. We tuned the hyperparameters of the FNN, e.g., the learning rate, and the network architecture individually in each scenario. Surprisingly, the CO-enriched ML pipeline including the FNN does not outperform the pipeline including the linear predictor in all scenarios: In scenarios with a small vehicle fleet size the linear predictor leads to better performance. This is due to an overfitting issue of the FNN on the training data, which we detail in Appendix G. In all other scenarios, the FNN leads to a slightly better performance.

Result 6. *The FNN predictor in the ML-layer improves the performance of the CO-enriched ML pipeline in most scenarios. However, the CO-enriched ML pipeline including the FNN does not generalize well for all scenarios.*

6. Conclusion

In this paper, we introduced a new family of online control policies for dispatching and rebalancing decisions in AMoD fleets. To derive such policies, we presented a novel CO-enriched ML pipeline that learns prescriptive dispatching and rebalancing decisions from full-information solutions. To establish this pipeline for our particular application case, we showed how to solve the underlying CO problem in polynomial time, how to leverage SL to learn a parametrization for the CO problem such that it allows for prescriptive dispatching and rebalancing actions, and how to derive corresponding learning-based control policies.

We presented a profound numerical study based on a real-world case study for Manhattan to show the efficacy of our learning-based policies and benchmark them against current state-of-the-art approaches: a greedy policy and a sampling-based receding horizon approach (cf. Alonso-Mora et al. 2017). Our results show that the sampling policy has an unstable performance and oftentimes performs even worse than the greedy policy. The performance of the sampling policy is in line with the performance of other benchmarks, e.g., DRL algorithms, that reach an improvement of up to 5% over myopic policies in similar settings. Our learning-based policies show a significant improvement over such approaches, yielding improvements over a greedy policy of up to 17.1%. Moreover, our learning-based policies are robust and always outperform the greedy policy. Finally, our learning-based policies yield a good trade-off between anticorrelated key performance indicators, e.g., when maximizing the total profit or the number of served customers, we still obtain a lower distance driven per vehicle compared to policies that show worse performance on the aforementioned quantities.

Acknowledgments

This work was supported by the German Research Foundation (DFG) under grant no. 449261765.

A. Fenchel-Young loss

When summarizing the results from Berthet et al. (2020),

$$F = \mathbb{E} \left[\max_{y \in \mathcal{Y}(x_i)} (\theta + Z)^T y \right] \quad (\text{A.1})$$

is strictly convex, twice differentiable, and has a gradient of

$$\nabla_{\theta} F = \mathbb{E} \left[\arg \max_{y \in \mathcal{Y}(x_i)} (\theta + Z)^T y \right]. \quad (\text{A.2})$$

When F is strictly convex, we can argue that $L(\theta, x_i, y_i^*)$ is also strictly convex as it is the sum of convex functions with at least one function being strictly convex. Then we can derive the gradient from

$$L(\theta, x_i, y_i^*) = \mathbb{E} \left[\max_{y \in \mathcal{Y}(x_i)} (\theta + Z)^T y \right] - \theta^T y_i^* \quad (\text{A.3})$$

as

$$\nabla_{\theta} L(\theta, x_i, y_i^*) := \mathbb{E} \left[\arg \max_{y \in \mathcal{Y}(x_i)} (\theta + Z)^T y \right] - y_i^*. \quad (\text{A.4})$$

B. Learning the ML-predictor φ_w for the case study

In this section, we describe how to learn the ML-predictor φ_w , which predicts the weights θ of digraph D in the ML-layer for the real-world case study. In our training set, we consider the weekdays 7th till 13th of January. For each day, we consider the time between 9:00 AM and 10:00 AM. To derive the target solutions for this training set, we apply the full-information approach to the problem comprising the surrounding time period from 8:30 AM to 10:30 AM. We use this surrounding time period to provide some time for balancing the system. Thereafter we extract the optimal full-information solution every four minutes between 9:00 AM and 10:00 AM and use the solution to rebuild the corresponding CO-layer-digraph solution. Then, the CO-layer-digraph object x_i and the CO-layer-digraph solution y_i^* form a training instance (x_i, y_i^*) . As we consider 5 days and a 1 hour interval with instances every four minutes we receive 80 training instances. Moreover, we draw 50 vectors with samples from a normal distribution $Z \sim \mathcal{N}(0, 1)$ to perturb the weight vector θ in the loss function (3.5) which we do by perturbing parameter vector w . Accordingly, evaluating the learning problem (3.3) in one learning iteration requires solving 80×50 instances of k -dSPPs. With the training data set, we solve the sample average approximation of the learning problem (3.3) using a BFGS algorithm. We detail the numerical values of parameter vector w that we used in SB and CB policies in Appendix C.

C. The feature vector

In this section, we detail the feature vector $\phi(\cdot)$. We manually selected the feature vector $\phi(\cdot)$ according to the best performance on a validation data set. We did not apply any further feature selection process as the perturbation of the parameter w during training acts as regularization and therefore automatically sets the parameter w of irrelevant features equal to zero. In Table 2, we present the learned parameters w for the SB policy, and in Table 3 we present the learned parameters w for the CB policy for its respective features $\phi(\cdot)$. Note that the respective values are only partially interpretable due to different feature scales. For the SB policy we did not normalize features before training as we achieved the best results without normalization, but for the CB policy we obtained the best results when normalizing features with its standard deviation.

The following parameters describe the rebalancing cell where the vehicle starts.					
parameter description		w_k	parameter description		w_k
0	num. of vehicles	1.091	4	est. num. of future starting requests	-0.229
1	num. of requests	0.0	5	est. num. of future arriving requests	0.854
2	num. of requests / num. of vehicles	-0.005	6	est. num. of future starting vehicles	0.022
3	num. of vehicles / num. of requests	0.101	7	est. num. of future arriving vehicles	0.019
The following parameters describe the rebalancing cell where the ride request starts.					
parameter description		w_k	parameter description		w_k
0	num. of vehicles	0.032	4	est. num. of future starting requests	0.021
1	num. of requests	0.005	5	est. num. of future arriving requests	0.02
2	num. of requests / num. of vehicles	0.001	6	est. num. of future starting vehicles	0.007
3	num. of vehicles / num. of requests	0.03	7	est. num. of future arriving vehicles	0.005
The following parameters describe the ride request.					
parameter description		w_k	parameter description		w_k
0	duration of tour	1.844	17	est. fut. rew. at d.off loc. + [16,18)min	0.099
1	reward of tour / duration of tour	0.007	18	est. fut. rew. at d.off loc. + [18,20)min	0.082
2	distance of tour	0.007	19	est. fut. rew. at d.off loc. + [20,22)min	0.071
3	reward of tour / distance of tour	0.883	20	est. fut. rew. at d.off loc. + [22,24)min	0.067
4	reward of tour / time till pick-up	0.295	21	est. fut. rew. at d.off loc. + [24,26)min	0.06
5	reward of tour / time till drop-off	0.006	22	est. fut. rew. at d.off loc. + [26,28)min	0.054
6	cost for tour / duration of tour	0.001	23	est. fut. rew. at d.off loc. + [28,30)min	0.05
7	costs for tour / time till drop-off	0.001	24	est. fut. rew. at d.off loc. + [30,32)min	0.047
8	reward for tour	3.115	25	est. fut. rew. at d.off loc. + [32,34)min	0.044
9	est. fut. rew. at d.off loc. + [0,2)min	0.611	26	est. fut. rew. at d.off loc. + [34,36)min	0.042
10	est. fut. rew. at d.off loc. + [2,4)min	0.853	27	est. fut. rew. at d.off loc. + [36,38)min	0.042
11	est. fut. rew. at d.off loc. + [4,6)min	0.59	28	est. fut. rew. at d.off loc. + [38,40)min	0.042
12	est. fut. rew. at d.off loc. + [6,8)min	0.301	29	est. fut. rew. at d.off loc. + [40,42)min	0.042
13	est. fut. rew. at d.off loc. + [8,10)min	0.204	30	est. fut. rew. at d.off loc. + [42,44)min	0.041
14	est. fut. rew. at d.off loc. + [10,12)min	0.17	31	est. fut. rew. at d.off loc. + [44,46)min	0.042
15	est. fut. rew. at d.off loc. + [12,14)min	0.141	32	est. fut. rew. at d.off loc. + [46,48)min	0.042
16	est. fut. rew. at d.off loc. + [14,16)min	0.116	33	est. fut. rew. at d.off loc. + [48,50)min	0.042
The following parameters describe the tour from the vehicle location to the ride request location.					
parameter description		w_k	parameter description		w_k
0	distance to request	-0.009	15	est. fut. cost at d.off loc. + [20,22)min	0.116
1	duration to request	-0.505	16	est. fut. cost at d.off loc. + [22,24)min	-0.7
2	cost for tour / duration of tour	0.0	17	est. fut. cost at d.off loc. + [24,26)min	-0.676
3	cost for tour / time till drop-off	0.0	18	est. fut. cost at d.off loc. + [26,28)min	-0.63
4	cost for tour / distance to request	0.256	19	est. fut. cost at d.off loc. + [28,30)min	-0.472
5	est. fut. cost at d.off loc. + [0,2)min	0.439	20	est. fut. cost at d.off loc. + [30,32)min	-0.47
6	est. fut. cost at d.off loc. + [2,4)min	-0.203	21	est. fut. cost at d.off loc. + [32,34)min	-0.352
7	est. fut. cost at d.off loc. + [4,6)min	-0.309	22	est. fut. cost at d.off loc. + [34,36)min	-0.31
8	est. fut. cost at d.off loc. + [6,8)min	-1.419	23	est. fut. cost at d.off loc. + [36,38)min	-0.352
9	est. fut. cost at d.off loc. + [8,10)min	-1.81	24	est. fut. cost at d.off loc. + [38,40)min	-0.484
10	est. fut. cost at d.off loc. + [10,12)min	-1.048	25	est. fut. cost at d.off loc. + [40,42)min	-0.483
11	est. fut. cost at d.off loc. + [12,14)min	-0.754	26	est. fut. cost at d.off loc. + [42,44)min	-0.484
12	est. fut. cost at d.off loc. + [14,16)min	-0.286	27	est. fut. cost at d.off loc. + [44,46)min	-0.548
13	est. fut. cost at d.off loc. + [16,18)min	0.106	28	est. fut. cost at d.off loc. + [46,48)min	-0.578
14	est. fut. cost at d.off loc. + [18,20)min	0.396	29	est. fut. cost at d.off loc. + [48,50)min	-0.582

Table 2: All parameters with its respective w values listed for the SB policy when optimizing over profit; fleet size: 2000; request density: 0.3.

The following parameters describe the rebalancing cell where the vehicle starts.					
parameter description	w_k		parameter description	w_k	
0	num. of vehicles	-0.048	4	est. num. of future starting requests	-0.859
1	num. of requests	0.302	5	est. num. of future arriving requests	1.018
2	num. of requests / num. of vehicles	-0.277	6	est. num. of future starting vehicles	0.2
3	num. of vehicles / num. of requests	-0.481	7	est. num. of future arriving vehicles	0.742
The following parameters describe the rebalancing cell where the ride request starts.					
parameter description	w_k		parameter description	w_k	
0	num. of vehicles	2.461	4	est. num. of future starting requests	3.047
1	num. of requests	3.462	5	est. num. of future arriving requests	2.629
2	num. of requests / num. of vehicles	5.924	6	est. num. of future starting vehicles	3.394
3	num. of vehicles / num. of requests	2.477	7	est. num. of future arriving vehicles	3.459
The following parameters describe the ride request.					
parameter description	w_k		parameter description	w_k	
0	duration of tour	3.922	5	reward of tour / time till drop-off	3.577
1	reward of tour / duration of tour	3.545	6	cost for tour / duration of tour	3.784
2	distance of tour	4.117	7	costs for tour / time till drop-off	3.815
3	reward of tour / distance of tour	3.501	8	reward for tour	3.867
4	reward of tour / time till pick-up	4.956			
The following parameters describe the tour from the vehicle location to the ride request location.					
parameter description	w_k		parameter description	w_k	
0	distance to request	-0.3	3	cost for tour / time till drop-off	0.022
1	duration to request	-1.216	4	cost for tour / distance to request	3.473
2	cost for tour / duration of tour	-0.26			
The following parameters describe a rebalancing location					
parameter description	w_k		parameter description	w_k	
0	num. of vehicles	-0.077	7	est. num. of future arriving vehicles	0.378
1	num. of requests	0.088	8	duration of tour	0.511
2	num. of requests / num. of vehicles	-0.362	9	reward of tour / duration of tour	-1.121
3	num. of vehicles / num. of requests	0.042	10	distance of tour	-0.618
4	est. num. of future starting requests	1.658	11	reward of tour / distance of tour	0.863
5	est. num. of future arriving requests	-0.017	12	cost for tour / duration of tour	0.756
6	est. num. of future starting vehicles	0.133	13	reward for tour	-0.468
The following parameters describe the tour to a rebalancing cell.					
parameter description	w_k		parameter description	w_k	
0	distance to location	-0.886	1	duration to location	-0.347
The following parameters describe the capacity vertices and its rebalancing cell.					
parameter description	w_k		parameter description	w_k	
0	num. of vehicles	-0.24	8	duration of tour	0.706
1	num. of requests	0.243	9	reward of tour / duration of tour	-1.407
2	num. of requests / num. of vehicles	-0.619	10	distance of tour	-0.761
3	num. of vehicles / num. of requests	0.076	11	reward of tour / distance of tour	1.208
4	est. num. of future starting requests	4.469	12	cost for tour / duration of tour	0.904
5	est. num. of future arriving requests	-0.051	13	reward for tour	-0.613
6	est. num. of future starting vehicles	0.244	14	idx of capacity vertex in reb. cell	-50.121
7	est. num. of future arriving vehicles	0.674			

Table 3: All parameters with its respective w values listed for the CB policy when optimizing over profit; fleet size: 2000; request density: 0.3.

D. Sparsification of the full-information digraph

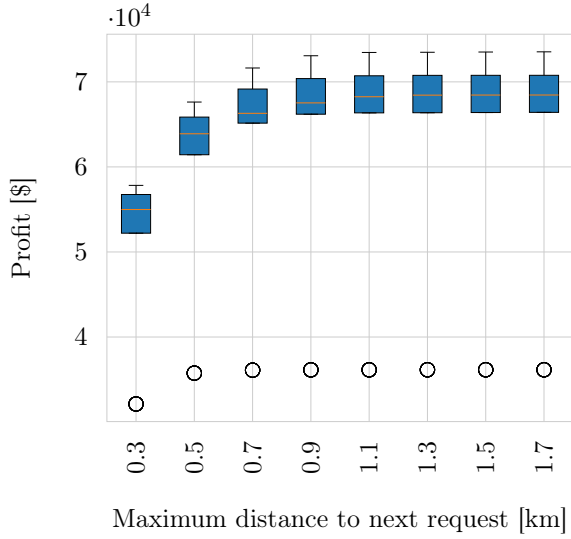


Figure 12: Spatial sparsification when optimizing the full-information bound over profit; fleet size: 2000; request density: 0.3.

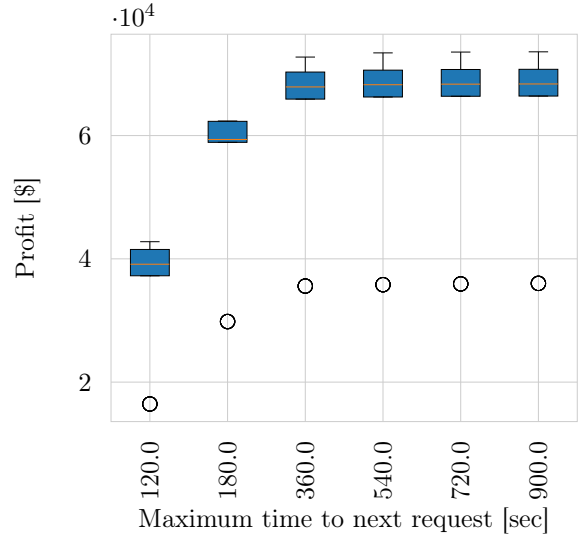


Figure 13: Temporal sparsification when optimizing the full-information bound over profit; fleet size: 2000; request density: 0.3.

The CO-layer-problem is solvable in polynomial time as a k -dSPP. Still, the computation time in real-world scenarios is crucial as the central controller only has limited time to make dispatching and rebalancing decisions in each system time period. Therefore, we sparsify the CO-layer-digraph D using temporal and spatial sparsification.

For temporal sparsification, we exclude arcs from the CO-layer-digraph D if a vehicle has a downtime greater than t^{\max} seconds, which is the case when a previous request r_i and the subsequent request r_j are more than t^{\max} apart from each other, $(s_{r_j} - a_{r_i} > t^{\max})$, or if a vehicle v has a downtime larger than t^{\max} to the first request r_i , $(s_{r_i} - t_v > t^{\max})$. We call this a temporal cut.

For spatial sparsification, we exclude arcs from the CO-layer-digraph D if a vehicle has to drive a distance further than d^{\max} to the next request, which is the case when a previous request r_i and the subsequent request r_j have a distance greater than d^{\max} , $\tau(d_{r_i}, o_{r_j}) > d^{\max}$, or if a vehicle v has to drive a distance greater than d^{\max} to the first request r_i , $\tau(l_v, o_{r_i}) > d^{\max}$. We call this a spatial cut.

Figure 12 and Figure 13 show that the sparsification of the graph with a spatial cut at 1.5 kilometers and a temporal cut at 720.0 seconds has no impact on the performance of the algorithm. We use these spatial and temporal cut values in our case study.

E. Hyperparameter selection for the sampling policy

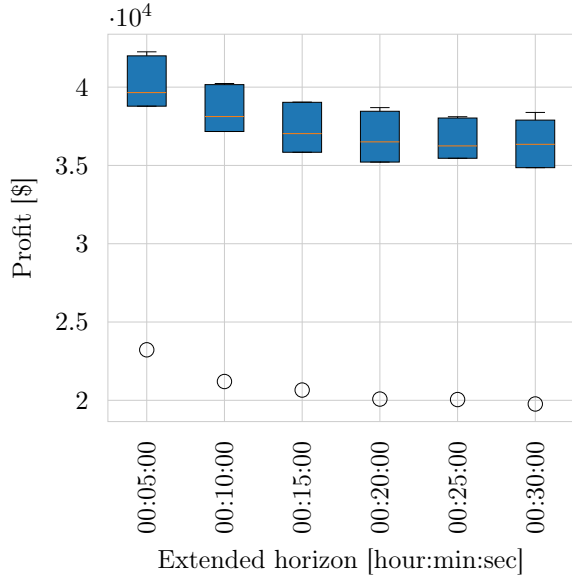


Figure 14: Performance of the sampling policy for different extended horizons when optimizing over profit. Fleet size: 2000; request density: 0.3.

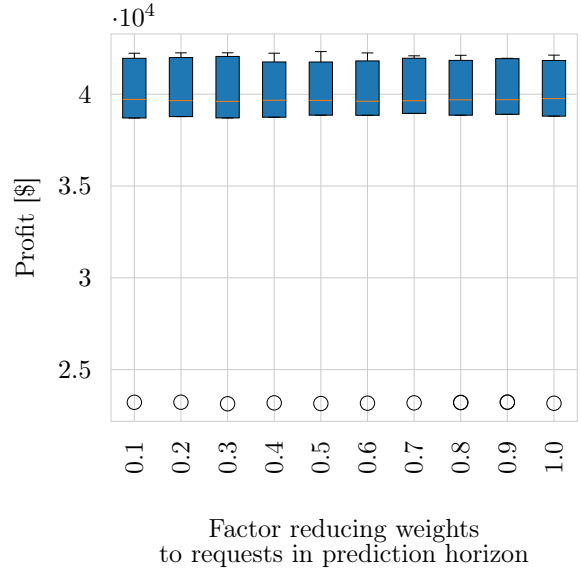


Figure 15: Performance of the sampling policy for different discount factors when optimizing over profit. Fleet size: 2000; request density: 0.3.

The performance of the sampling policy depends on the sampled requests in the prediction horizon. Therefore we investigate different lengths of the prediction horizon to determine the best prediction horizon length (see Figure 14). We choose a prediction horizon of four minutes as we achieved the best results with this setting on a validation data set. We recall that the prediction horizon is the extended horizon minus the system time period of one minute.

Moreover, the sampling policy improves performance when preferring requests in the system time period over requests in the prediction horizon according to Alonso-Mora et al. (2017). Therefore we test the sampling policy over different discount factors for sampled requests (Figure 15). The discount factor is a multiplication factor that we use to reduce weights on arcs to sampled requests in the prediction horizon. We choose a discount factor of 0.2 as we received the best results for this setting on a validation data set.

F. Hyperparameter selection for the variants SP and CP of the CO-enriched ML pipeline

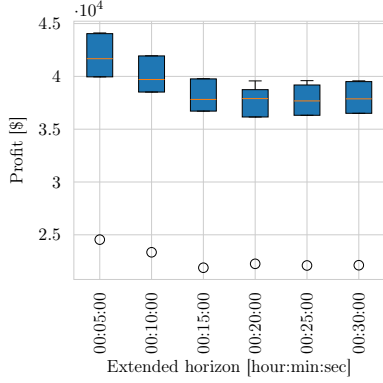


Figure 16: SB policy for different extended horizons when optimizing over profit. Fleet size: 2000; request density: 0.3.

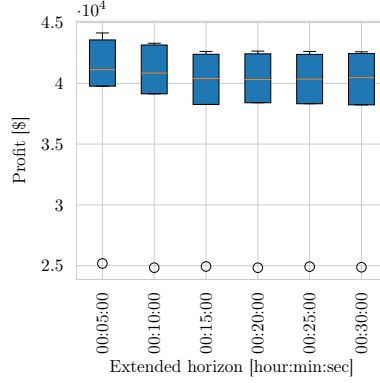


Figure 17: CB policy for different extended horizons when optimizing over profit. Fleet size: 2000; request density: 0.3.

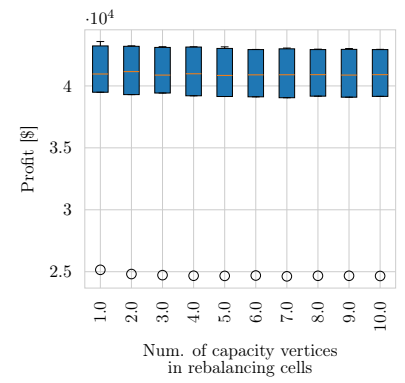


Figure 18: CB policy for different number of capacity vertices in rebalancing cells. Fleet size: 2000; request density: 0.3.

In this section, we determine the hyperparameters for the CO-enriched ML pipeline variants, namely the SB and CB policies. We tested the SB policy (Figure 16) and the CB policy (Figure 17) with different prediction horizons. For the SB and CB policy a prediction horizon of four minutes performs best when testing on a validation data set. We recall that the prediction horizon is the extended horizon minus the system time period of one minute. We tested the CB policy with different amounts of capacity vertices for each rebalancing cell (Figure 18). We retrieved the best performance with one capacity vertex for each rebalancing cell when testing on a validation data set.

G. Comparing the performance of the deep learning ML-layer and the linear ML-layer

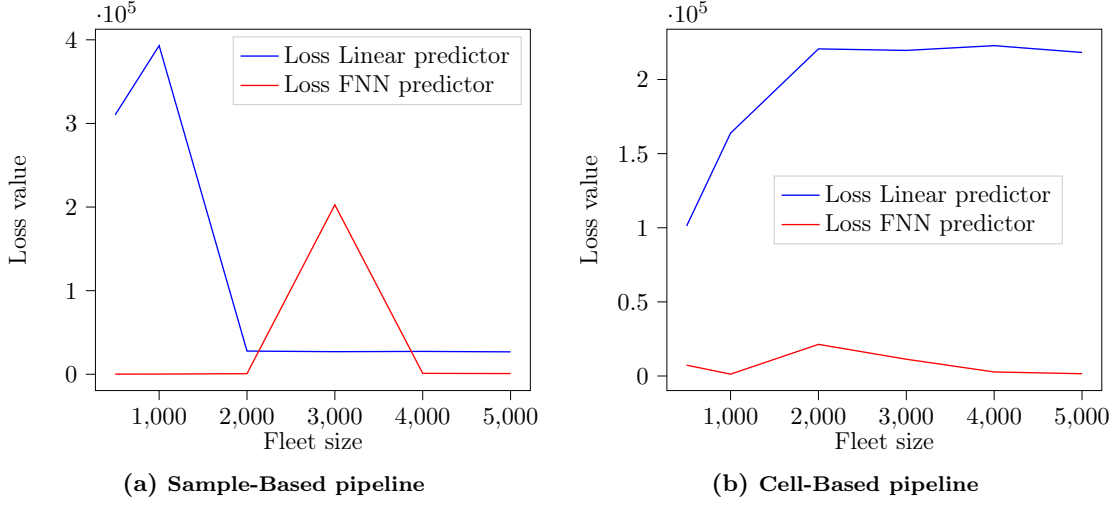


Figure 19: Comparison of loss value with FNN predictor and linear predictor for different fleet sizes.

In Figure 19 we compare the Fenchel-Young loss values of the CO-enriched ML pipeline at the end of training for an FNN predictor and a linear predictor in the ML-layer. Apart from the outlier in the SB setting with a fleet size of 3000 for which the FNN has not converged after 70 hours of training, we can see that the loss is always smaller for the FNN predictor. The lower loss value when using the FNN predictor shows that, as expected, the FNN better approximates the true cost function of the CO-layer-digraph and therefore leads to better results on almost all scenarios (Figure 11).

However, the better loss value does not necessarily lead to better generalization: in some scenarios, the CO-enriched ML pipeline using an FNN predictor does not outperform the pipeline using the linear predictor (Figure 11). Figure 20 shows why this is the case by comparing the difference between \hat{y}_i and y_i^* on the training set $(x_1, y_1^*), \dots, (x_n, y_n^*)$. Here, $g_{FNN} = \sum(\hat{y}_{i,FNN} == y_i^*)$ and $g_{Linear} = \sum(\hat{y}_{i,Linear} == y_i^*)$ indicate the number of matching edges in the predicted solution \hat{y}_i and the true solution y_i^* , using the FNN predictor and the linear predictor, respectively. In scenarios where the CO-enriched ML pipeline using the FNN predictor performs worse than the pipeline using the linear predictor (Figure 11) during testing, the FNN predictor still outperforms the linear model ($g_{FNN} > g_{Linear}$) on the training set. This indicates that the FNN predictor is overfitting in these scenarios.

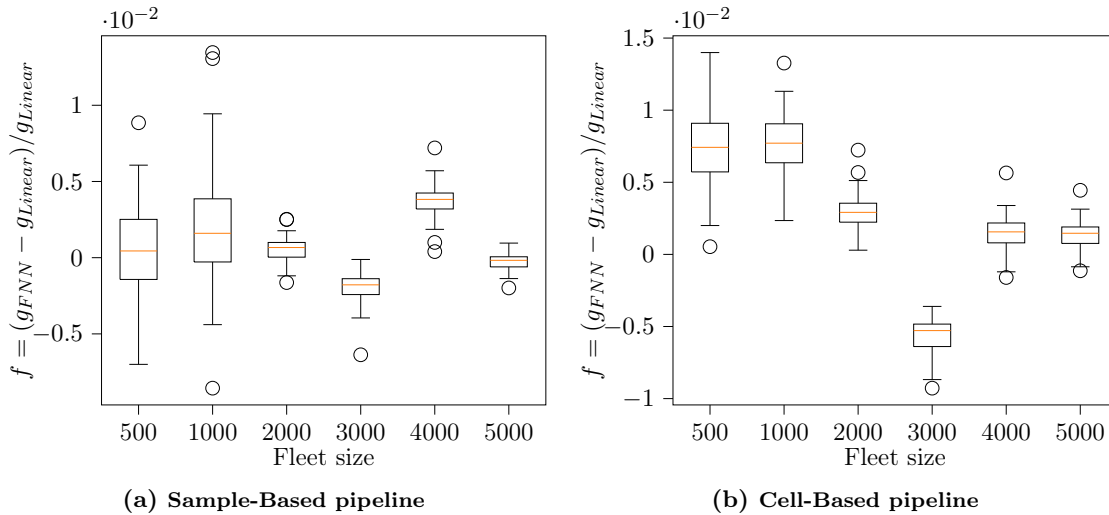


Figure 20: Comparison of equality between \hat{y}_i and y_i^* on all instances i in training set $(x_1, y_1^*), \dots, (x_n, y_n^*)$.

References

- Alonso-Mora, J., Wallar, A., & Rus, D. (2017). Predictive routing for autonomous mobility-on-demand systems with ride-sharing. In *2017 IEEE/RSJ International Conference on Intelligent Robots and Systems (IROS)* (pp. 3583–3590). doi:10.1109/IROS.2017.8206203.
- Bengio, Y., Lodi, A., & Prouvost, A. (2021). Machine learning for combinatorial optimization: A methodological tour d’horizon. *European Journal of Operational Research*, *290*, 405–421. URL: <https://www.sciencedirect.com/science/article/pii/S0377221720306895>. doi:<https://doi.org/10.1016/j.ejor.2020.07.063>.
- Berthet, Q., Blondel, M., Teboul, O., Cuturi, M., Vert, J.-P., & Bach, F. (2020). Learning with differentiable perturbed optimizers. In H. Larochelle, M. Ranzato, R. Hadsell, M. Balcan, & H. Lin (Eds.), *Advances in Neural Information Processing Systems* (pp. 9508–9519). Curran Associates, Inc. volume 33. URL: <https://proceedings.neurips.cc/paper/2020/file/6bb56208f672af0dd65451f869fedfd9-Paper.pdf>.
- Bertsimas, D., Jaillet, P., & Martin, S. (2019). Online vehicle routing: The edge of optimization in large-scale applications. *Operations Research*, *67*, 143–162. doi:10.1287/opre.2018.1763.
- Bösch, P. M., Becker, F., Becker, H., & Axhausen, K. W. (2018). Cost-based analysis of autonomous mobility services. *Transport Policy*, *64*, 76–91. doi:10.1016/j.tranpol.2017.09.005.
- Dalle, G., Baty, L., Bouvier, L., & Parmentier, A. (2022). Learning with combinatorial optimization layers: a probabilistic approach. *arXiv preprint arXiv:2207.13513*, .
- Donti, P., Amos, B., & Kolter, J. Z. (2017). Task-based end-to-end model learning in stochastic optimization. In I. Guyon, U. V. Luxburg, S. Bengio, H. Wallach, R. Fergus, S. Vishwanathan, & R. Garnett (Eds.), *Advances in Neural Information Processing Systems*. Curran Associates, Inc. volume 30. URL: <https://proceedings.neurips.cc/paper/2017/file/3fc2c60b5782f641f76bcefc39fb2392-Paper.pdf>.
- Elmachtoub, A. N., & Grigas, P. (2022). Smart “predict, then optimize”. *Management Science*, *68*, 9–26. URL: <https://doi.org/10.1287/mnsc.2020.3922>. doi:10.1287/mnsc.2020.3922.
- Enders, T., Harrison, J., Pavone, M., & Schiffer, M. (2023). Hybrid multi-agent deep reinforcement learning for autonomous mobility on demand systems. In N. Matni, M. Morari, & G. J. Pappas (Eds.), *Proceedings of the 5th Annual Learning for Dynamics and Control Conference* (pp. 1284–1296). PMLR volume 211 of *Proceedings of Machine Learning Research*. URL: <https://proceedings.mlr.press/v211/enders23a.html>.
- Gammelli, D., Yang, K., Harrison, J., Rodrigues, F., Pereira, F. C., & Pavone, M. (2021). Graph neural network reinforcement learning for autonomous mobility-on-demand systems. In *2021 60th IEEE Conference on Decision and Control (CDC)* (pp. 2996–3003). doi:10.1109/CDC45484.2021.9683135.
- Iglesias, R., Rossi, F., Wang, K., Hallac, D., Leskovec, J., & Pavone, M. (2018). Data-driven model predictive control of autonomous mobility-on-demand systems. In *2018 IEEE International Conference on Robotics and Automation (ICRA)* (pp. 6019–6025). doi:10.1109/ICRA.2018.8460966.

- Jiao, Y., Tang, X., Qin, Z. T., Li, S., Zhang, F., Zhu, H., & Ye, J. (2021). Real-world ride-hailing vehicle repositioning using deep reinforcement learning. *Transportation Research Part C: Emerging Technologies*, *130*, 103289. URL: <https://www.sciencedirect.com/science/article/pii/S0968090X21003004>. doi:<https://doi.org/10.1016/j.trc.2021.103289>.
- Kotary, J., Fioretto, F., Van Hentenryck, P., & Wilder, B. (2021). End-to-end constrained optimization learning: A survey. In Z.-H. Zhou (Ed.), *Proceedings of the Thirtieth International Joint Conference on Artificial Intelligence, IJCAI-21* (pp. 4475–4482). International Joint Conferences on Artificial Intelligence Organization. URL: <https://doi.org/10.24963/ijcai.2021/610>. doi:10.24963/ijcai.2021/610 survey Track.
- Levy, J. I., Buonocore, J. J., & Stackelberg, K. V. (2010). Evaluation of the public health impacts of traffic congestion: A health risk assessment. *Environmental Health: A Global Access Science Source*, *9*. doi:10.1186/1476-069X-9-65.
- Li, M., Qin, Z., Jiao, Y., Yang, Y., Wang, J., Wang, C., Wu, G., & Ye, J. (2019). Efficient ridesharing order dispatching with mean field multi-agent reinforcement learning. In *The World Wide Web Conference WWW '19* (p. 983–994). New York, NY, USA: Association for Computing Machinery. URL: <https://doi.org/10.1145/3308558.3313433>. doi:10.1145/3308558.3313433.
- Liang, E., Wen, K., Lam, W. H. K., Sumalee, A., & Zhong, R. (2022). An integrated reinforcement learning and centralized programming approach for online taxi dispatching. *IEEE Transactions on Neural Networks and Learning Systems*, *33*, 4742–4756. doi:10.1109/TNNLS.2021.3060187.
- Liu, Y., & Samaranyake, S. (2022). Proactive rebalancing and speed-up techniques for on-demand high capacity ridesourcing services. *IEEE Transactions on Intelligent Transportation Systems*, *23*, 819–826. doi:10.1109/TITS.2020.3016128.
- Nowozin, S., & Lampert, C. H. (2010). Structured learning and prediction in computer vision. *Foundations and Trends in Computer Graphics and Vision*, *6*, 185–365. doi:10.1561/06000000033.
- NYC Taxi & Limousine Commission (2015). New York City Taxi & Limousine Commission - TLC Trip Record Data. URL: <https://www1.nyc.gov/site/tlc/about/tlc-trip-record-data.page>.
- Parmentier, A. (2021). Learning to approximate industrial problems by operations research classic problems. *Operations Research*, . doi:10.1287/opre.2020.2094.
- Parmentier, A., & T'Kindt, V. (2022). Structured learning based heuristics to solve the single machine scheduling problem with release times and sum of completion times. *European Journal of Operational Research*, . URL: <https://www.sciencedirect.com/science/article/pii/S0377221722005148>. doi:<https://doi.org/10.1016/j.ejor.2022.06.040>.
- Pavone, M. (2015). Autonomous mobility-on-demand systems for future urban mobility. In *Autonomes Fahren: Technische, rechtliche und gesellschaftliche Aspekte* (pp. 399–416). Berlin, Heidelberg: Springer Berlin Heidelberg. URL: https://doi.org/10.1007/978-3-662-45854-9_19. doi:10.1007/978-3-662-45854-9_19.
- Pavone, M., Smith, S. L., Frazzoli, E., & Rus, D. (2012). Robotic load balancing for mobility-on-demand systems. *International Journal of Robotics Research*, *31*, 839–854. doi:10.1177/0278364912444766.
- Sadeghi Eshkevari, S., Tang, X., Qin, Z., Mei, J., Zhang, C., Meng, Q., & Xu, J. (2022). Reinforcement learning in the wild: Scalable rl dispatching algorithm deployed in ridehailing marketplace. In *Proceedings of the 28th ACM SIGKDD Conference on Knowledge Discovery and Data Mining KDD '22* (p. 3838–3848). New York, NY, USA: Association for Computing Machinery. URL: <https://doi.org/10.1145/3534678.3539095>. doi:10.1145/3534678.3539095.
- Schiffer, M., Hiermann, G., Rüdell, F., & Walther, G. (2021). A polynomial-time algorithm for user-based relocation in free-floating car sharing systems. *Transportation Research Part B: Methodological*, *143*, 65–85. doi:10.1016/j.trb.2020.11.001.
- Schrank, D., Eisele, B., & Lomax, T. (2019). *2019 Urban Mobility Report*. Technical Report Texas A&M Transportation Institute. URL: <https://static.tti.tamu.edu/tti.tamu.edu/documents/mobility-report-2019.pdf>.
- Skordilis, E., Hou, Y., Tripp, C., Moniot, M., Graf, P., & Biagioni, D. (2022). A modular and transferable reinforcement learning framework for the fleet rebalancing problem. *IEEE Transactions on Intelligent Transportation Systems*, *23*, 11903–11916. doi:10.1109/TITS.2021.3108733.
- Statista (2021). Market share of the leading ride-hailing companies in the united states from september 2017 to july 2021. URL: <https://www.statista.com/statistics/910704/market-share-of-rideshare-companies-united-states/>.
- Tang, X., Qin, Z. T., Zhang, F., Wang, Z., Xu, Z., Ma, Y., Zhu, H., & Ye, J. (2019). A deep value-network based approach for multi-driver order dispatching. In *Proceedings of the 25th ACM SIGKDD International Conference on Knowledge Discovery & Data Mining KDD '19* (p. 1780–1790). New York, NY, USA: Association for Computing Machinery. URL: <https://doi.org/10.1145/3292500.3330724>. doi:10.1145/3292500.3330724.

-
- Tsao, M., Iglesias, R., & Pavone, M. (2018). Stochastic Model Predictive Control for Autonomous Mobility on Demand. In *IEEE Conference on Intelligent Transportation Systems, Proceedings, ITSC* (pp. 3941–3948). volume 2018-Novem. doi:10.1109/ITSC.2018.8569459. arXiv:1804.11074.
- Vidal, T., Laporte, G., & Matl, P. (2020). A concise guide to existing and emerging vehicle routing problem variants. *European Journal of Operational Research*, 286, 401–416. URL: <https://www.sciencedirect.com/science/article/pii/S0377221719308422>. doi:<https://doi.org/10.1016/j.ejor.2019.10.010>.
- White, J. (2020). Waymo opens driverless robo-taxi service to the public in phoenix. *Reuters*, . URL: <https://www.reuters.com/article/us-waymo-autonomous-phoenix-idUKKBN26T2Y3>.
- Xu, Z., Li, Z., Guan, Q., Zhang, D., Li, Q., Nan, J., Liu, C., Bian, W., & Ye, J. (2018). Large-scale order dispatch in on-demand ride-hailing platforms: A learning and planning approach. In *Proceedings of the 24th ACM SIGKDD International Conference on Knowledge Discovery & Data Mining KDD '18* (p. 905–913). New York, NY, USA: Association for Computing Machinery. URL: <https://doi.org/10.1145/3219819.3219824>. doi:10.1145/3219819.3219824.
- Zardini, G., Lanzetti, N., Pavone, M., & Frazzoli, E. (2022). Analysis and control of autonomous mobility-on-demand systems. *Annual Review of Control, Robotics, and Autonomous Systems*, 5, 633–658. URL: <https://doi.org/10.1146/annurev-control-042920-012811>. doi:10.1146/annurev-control-042920-012811. arXiv:<https://doi.org/10.1146/annurev-control-042920-012811>.
- Zhang, R., & Pavone, M. (2016). Control of robotic mobility-on-demand systems: A queueing-theoretical perspective. *International Journal of Robotics Research*, 35, 186–203. doi:10.1177/0278364915581863. arXiv:1404.4391.
- Zhou, M., Jin, J., Zhang, W., Qin, Z., Jiao, Y., Wang, C., Wu, G., Yu, Y., & Ye, J. (2019). Multi-agent reinforcement learning for order-dispatching via order-vehicle distribution matching. In *Proceedings of the 28th ACM International Conference on Information and Knowledge Management CIKM '19* (p. 2645–2653). New York, NY, USA: Association for Computing Machinery. URL: <https://doi.org/10.1145/3357384.3357799>. doi:10.1145/3357384.3357799.